Title: Enteric helminths promote *Salmonella* co-infection by altering the intestinal metabolome

Running Title: Intestinal metabolites mediate co-infection

Authors: Lisa A. Reynolds[1,2], Stephen A. Redpath[3], Sophie Yurist-Doutsch[1], Navkiran Gill[1], Eric M. Brown[1,3], Joris van der Heijden[1,3], Tara P. Brosschot[1], Jun Han[4], Natalie C. Marshall[1,3], Sarah E. Woodward[1,3], Yanet Valdez[1], Christoph H. Borchers[2,4-6], Georgia Perona-Wright[3,7,*], B. Brett Finlay[1,3,8,*]

Affiliations:

[1] Michael Smith Laboratories, University of British Columbia, Vancouver, BC, V6T 1Z4, Canada.

[2] Department of Biochemistry and Microbiology, University of Victoria, Victoria, BC, V8P 5C2, Canada

[3] Department of Microbiology and Immunology, University of British Columbia, Vancouver, BC, V6T 1Z3, Canada.

[4] University of Victoria-Genome British Columbia Proteomics Centre, Victoria, BC, V8Z 7X8, Canada.

[5] Gerald Bronfman Department of Oncology, Jewish General Hospital, McGill University, Montreal, Quebec, H3T 1E2, Canada

[6] Proteomics Centre, Segal Cancer Centre, Lady Davis Institute, Jewish General Hospital, McGill University, Montreal, Quebec, H3T 1E2, Canada

[7] Institute of Infection Immunity and Inflammation, University of Glasgow, Glasgow, G12 8TA, United Kingdom.

[8] Department of Biochemistry and Molecular Biology, University of British Columbia, Vancouver, BC, V6T 1Z3, Canada.

[*] G.P-W. and B.B.F. contributed equally to this work.

Correspondence: bfinlay@mail.ubc.ca or georgia.perona-wright@glasgow.ac.uk

Article Summary for Table of Contents:

Intestinal helminth infection increases small intestinal colonization by *Salmonella*, which occurs independently of the induction of T regulatory or Th2 cells following helminth infection. Helminth infection disrupts the intestinal metabolome, and the resulting shift in metabolites directly enhances *Salmonella* virulence.

Abstract: Intestinal helminth infections occur predominantly in regions where exposure to enteric bacterial pathogens is also common. Helminth infections inhibit host immunity against microbial pathogens, which has largely been attributed to the induction of regulatory or type 2 (Th2) immune responses. Here we demonstrate an additional three-way interaction in which helminth infection alters the metabolic environment of the host intestine to enhance bacterial pathogenicity. We show that an ongoing helminth infection increased colonization by *Salmonella* independently of T regulatory or Th2 cells. Instead, helminth infection altered the metabolic profile of the intestine, which directly enhanced bacterial expression of *Salmonella* pathogenicity island 1 (SPI-1) genes and increased intracellular invasion. These data reveal a novel mechanism by which a helminth-modified metabolome promotes susceptibility to bacterial co-infection.

Word count: 123

Keywords: co-infection; immunomodulation; parasites; helminths; bacterial infection; intestinal metabolites

Background:

Chronic helminth infections occur predominantly in regions of poor sanitation, where the risk of co-infection with microbial pathogens is high [1]. Ongoing helminth infections have been associated with increased susceptibility to secondary microbial infections in mice and people. In mice, helminths impair host resistance to *Citrobacter rodentium*, *Salmonella enterica* serovar Typhimurium, *Escherichia coli* strain UTI89 (UPEC), norovirus and *y*-herpesvirus [2–6]. In humans, helminth infections correlate with increased severity of tuberculosis, higher *Plasmodium* burdens during malaria, impaired immunity to *Vibrio cholerae*, and greater incidence of human immunodeficiency virus (HIV) infection [7–12].

It is currently thought that helminth mediated immunomodulation underpins increased susceptibility to secondary microbial infections. Helminth infections characteristically induce a robust T helper (Th)2 immune response, marked by the cytokines IL-4, IL-5 and IL-13, and a strong regulatory T cell (Treg) response [13]. Both Th2 and Treg responses have been proposed to impair the generation of protective Th1 or Th17 immunity against bacterial or viral pathogens [2–5,14–16]. In this regard, widespread IL-4 signaling during helminth infection can impair the production of antimicrobial IFN-γ from $CD4^+$ T cells and invariant natural killer T cells [2,5,17], and helminth-elicited IL-4 and IL-10 can block effector differentiation of $CD8^+$ T cells after challenge with irradiated *Toxoplasma gondii* parasites [16]. Moreover, Th2 cytokines can directly promote viral replication: IL-4 switches on signal transducer and activator of transcription 6 (Stat6) which binds to and activates γ-herpes viral promotors controlling latent-lytic switch genes [4]. Alongside Th2 cytokines, Tregs can impede antimicrobial immunity through the suppression of effector T cell responses [14,15]. In this manner, helminth-induced Tregs can also reduce inflammation during allergic airway inflammation and graft versus host

disease [18–20]. Thus, direct modulation of host immunity is one pathway by which helminths facilitate secondary microbial infections.

Here, we use a mouse model of co-infection to identify an additional mechanism by which intestinal helminths alter host immunity to concurrent bacterial pathogens. We show that the greater susceptibility of helminth-infected mice to the bacterial pathogen *S.* Typhimurium occurs independently of the induction of Treg or Th2 cells following helminth infection. Instead, we reveal a previously unidentified pathway of inter-kingdom interaction between helminths and bacteria. We show that helminths disrupt the metabolic profile of the small intestine, and that the resulting metabolites directly affect the virulence of *S.* Typhimurium to enhance bacterial colonization.

Methods:

Mice

All mouse experiments were performed at the University of British Columbia (UBC) and approved by UBC's Animal Care Committee and the Canadian Council on Animal Care. Wildtype C57BL/6 mice were purchased from the Jackson Laboratory, and wildtype 129S1/SvImJ, *rag1*$^{-/-}$, C57BL/6 4get [21], C57BL/6 KN2/KN2 (*il4*$^{-/-}$) [22] and C57BL/6 4get *stat6*$^{-/-}$ [23] mice were bred in-house. All mice were housed in individually ventilated cages in specific-pathogen-free conditions, with ad lib access to food and water. Experimental mice were age- and sex-matched and used at 6-12 weeks old. Littermates were randomized between test groups prior to the start of each experiment.

Infections

Mice were left naïve or infected by oral gavage with 200 *H. polygyrus* third stage larvae. Where indicated, naïve or day-14 *H. polygyrus*-infected mice were infected with streptomycin-resistant *Salmonella enterica* serovar Typhimurium wildtype or *aroA* mutant strain SL1344. 129S1/SvImJ mice were orally gavaged with 3 x 10^6 colony forming units (cfu) of stationary-phase *S.* Typhimurium in phosphate-buffered saline (PBS), from overnight cultures grown in LB broth. C57BL/6 mice were orally gavaged with 3 x 10^8 cfu of stationary-phase *aroA* mutant *S.* Typhimurium [24].

In vivo *Salmonella* burden quantification

Serial dilutions of homogenized tissues were plated onto LB plates containing 100 μg/mL streptomycin (Sigma-Aldrich). The following day, *S.* Typhimurium colonies were counted and cfu per gram of tissue was calculated.

Metabolite collection

Intestinal contents were collected from the proximal 6 cm of the small intestine of naïve or day-14 *H.* polygyrus-infected mice, and weights were recorded. 100 µL of acetonitrile (VWR) was added for each 10 mg of intestinal content, and samples were shaken at 4 °C overnight. Samples were spun at 13,000 rpm at 4 °C for 15 minutes, and supernatants containing small molecules were collected. Supernatants were sterile-filtered, aliquoted into 250 µL (containing 25 mg intestinal contents) fractions, and acetonitrile was evaporated using a speed vacuum concentrator. Samples were stored at -80 °C prior to the use of metabolites for compositional analysis or functional assays. Control tubes were generated where acetonitrile was used as above to do mock extractions in an empty tube.

Metabolite analysis

In brief, metabolites were extracted as above from naïve or day-14 *H. polygyrus*-infected 129S1/SvImJ mice and sent to the University of Victoria-Genome BC Proteomics Centre for untargeted metabolomics by Ultrahigh-Performance Liquid Chromatography-Fourier transform mass spectrometry (UPLC-FTMS) analysis. The positive ion and negative ion UPLC-FTMS datasets were processed individually, and the output of the data processing was the retention time, mass-to-charge ratio (m/z) and peak area of each detected metabolite or metabolite feature. Welch t-test with unequal variances was applied for the statistical analysis. Multivariate and clustering analyses were carried out using Metaboanalyst version 3.0 software (http://www.metaboanalyst.ca/faces/home.xhtml) [25,26], using a m/z tolerance of 0.0005 and a retention time tolerance of 30 seconds. Data were log transformed and auto scaled. Principal component analysis (PCA) was performed and plots were generated showing separation of data based on the first two principal components. Heat maps were generated showing relative abundance of all small intestinal metabolites. Maximum abundance was reported in red and

minimum abundance in blue. Clustering of samples from different mice was shown using a Euclidean distance and Ward clustering algorithm. Where possible, putative identities of identified metabolite features were assigned using the Metlin database (https://metlin.scripps.edu/metabo_batch.php) based on the m/z value of each feature. Statistical analyses were performed separately on datasets from positive and negative ion detection datasets. Full details are provided in the Supplementary Methods.

Incubation of *Salmonella* with intestinal metabolites

Mock extracted metabolites (control), metabolites from small intestinal contents of naïve mice, or metabolites from small intestinal contents of day-14 *H. polygyrus*-infected mice were resuspended in 1 mL of LB media and sterile-filtered using a 0.22 μM pore filter unit (Sigma-Aldrich). 30 μL of stationary-phase overnight cultures of *S.* Typhimurium or *aroA* mutant *S.* Typhimurium grown in LB were diluted into the 1 mL of LB containing metabolites, and shaken at 37 °C for 3 hours. *S.* Typhimurium was then pelleted and resuspended in PBS twice, to wash cells.

***S.* Typhimurium gene expression**

After incubation with metabolites as described above, *S.* Typhimurium was resuspended in RNAprotect Bacteria Reagent (Qiagen), and RNA was extracted using an RNeasy Mini Kit (Qiagen). Genomic DNA was removed using a DNA-Free™ kit (Ambion), and cDNA was prepared using a QuantiTect® Reverse Transcription Kit (Qiagen). Real-Time Quantitative PCR (qPCR) was performed on a 7500 Fast Real-Time PCR System (Applied Biosystems). Cycling conditions used were: 2 minutes at 50 °C, 15 minutes at 95 °C, followed by 40 cycles of 95 °C for 15 seconds, 58 °C for 30 seconds, 72 °C for 30 seconds. Primers used were (5'-3') *hilA*: F-ACACCTGCAGGATAATCCAA, R-ATTTTCGTGCCAGTTCATGT; *sipA*: F-

GTCATAATGCCAGGTATGCAGACCG, R-CCTTTAATTTCCCCTGACAGCGTCG; *sprB*: F-CATTAACTGCACTTTTGCATTCCCTATCCG, R-GCCACTACCAAAACTTTACGGTTCTGCA; and *glyceraldehyde-3-phosphate dehydrogenase* (*gapA*): F-GGCGCTAACTTTGACAAATACGAAGG, R-AGTCATCAGACCTTCGATGATGCCG. Normalized expression units of test genes were calculated using the Delta-Delta Ct method relative to *gapA*. Expression levels were normalized to that of the control group (*S.* Typhimurium cultured with mock extracted metabolites) which was set to an expression level of 1.

In vitro *S.* Typhimurium invasion assay

HeLa cells were purchased from the American Type Culture Collection (ATCC) and cultured in DMEM (HyClone) containing 10 % heat-inactivated FBS (HyClone), 1 % GlutaMAX (ThermoFisher) and 1 % non-essential amino acids (Gibco) (complete DMEM), at 37 °C with 5 % CO_2. Cultures of *S.* Typhimurium that had been incubated with intestinal metabolites (described above) were used to infect HeLa cells at a multiplicity of infection of 50. *S.* Typhimurium inoculates were plated on LB plates containing 100 μg/mL streptomycin (Sigma-Aldrich) to confirm the cfu of *S.* Typhimurium present in inoculates. Twenty minutes post-infection HeLa cells were washed with PBS, and complete DMEM containing 50 μg/mL gentamicin (Gold Biotechnology) was added. After a further 70 minute incubation, HeLa cells were lysed using PBS containing 1 % Triton X-100 (Sigma-Aldrich) and 0.1 % sodium dodecyl sulfate (SDS; Sigma-Aldrich). Serial dilutions of lysate were plated onto LB plates containing 100 μg/mL streptomycin (Sigma-Aldrich). The following day, *S.* Typhimurium colonies were counted and invasion level was calculated as the % of *S.* Typhimurium cfu present in inoculates that invaded HeLa cells. The control group (*S.* Typhimurium cultured with mock-extracted

metabolites) invasion level was set to 1, and invasion levels of other groups shown relative to this value.

Statistical analysis

Data were analysed for normality using a D'Agostino-Pearson omnibus normality test. For assessing differences between two groups, an unpaired t test was used for normally distributed data, and a Mann-Whitney test was used for data that were not normally distributed. When more than two test groups were being assessed, a one-way ANOVA followed by a Tukey's multiple comparisons test was used for normally distributed data, and a Kruskal-Wallis test followed by a Dunn's multiple comparisons test was used for data which were not normally distributed. A p value ≥ 0.05 was considered statistically significant. * = $p \leq 0.05$, ** = $p \leq 0.01$, *** = $p \leq 0.001$, **** = $p \leq 0.0001$, NS = not significant.

Results:

Helminth co-infected mice exhibit elevated *S.* Typhimurium burdens in the small intestine

To test the effects of intestinal helminth infection on bacterial co-colonization, we developed a model of co-infection using the murine helminth *Heligmosomoides polygyrus* and the bacteria *S.* Typhimurium. 129S1/SvImJ mice were orally infected with *H. polygyrus*, a strictly enteric pathogen which establishes a chronic infection in the small intestine [27]. At day fourteen following *H. polygyrus* infection, by which time adult worms are present in the lumen of the duodenum and jejunum, mice were orally challenged with *S.* Typhimurium, alongside mice infected with *S.* Typhimurium alone (Figure 1*A*). The majority of singly infected mice were able to clear *S.* Typhimurium from the small intestine within nine days, yet *H. polygyrus* co-infected mice maintained high bacterial burdens (Figure 1*B*). In the cecum and colon, sites distal to helminth infection, the effect of helminth co-infection on *S.* Typhimurium clearance was less marked, although helminth co-infection did result in significantly higher *S. T*yphimurium levels in the colon (Figure 1*C*). Levels of systemic *S.* Typhimurium were unaffected by helminth co-infection (Figure 1*D*). Together, this data suggests that *H. polygyrus* exerts a local effect to promote *S.* Typhimurium colonization.

To test if the effect of helminth infection on bacterial colonization was affected by genetic background, we also co-infected C57BL/6 mice (Figure 2*A*). Unlike 129S1/SvImJ mice, C57Bl/6 mice lack the natural resistance-associated macrophage protein 1 (Nramp1), and rapidly succumb to infection with doses of wildtype *S.* Typhimurium that 129S1/SvImJ mice survive [28]. For this reason, all experiments with C57BL/6 mice were conducted with an attenuated strain of *S.* Typhimurium (*aroA* mutant [24]). Similar to 129S1/SvImJ mice, C57BL/6 mice infected with *S.* Typhimurium alone were able to clear this pathogen from the small intestine within nine days,

whereas helminth co-infected mice maintained high *S.* Typhimurium burdens in the small intestine (Figure 2*B*). The greatest impact of helminth co-infection was at sites proximal to *H. polygyrus* colonization (Figure 2*C* and *D*). Notably, small intestinal bacterial burdens were significantly higher in helminth co-infected mice as early as 24 hours following *S.* Typhimurium infection (Figure 2*B*). Therefore, in two different inbred strains of mice, the presence of an intestinal helminth enhances local bacterial colonization following challenge infection.

Elevated *S.* Typhimurium burdens in helminth co-infected mice are independent of induction of Th2 or Treg cells

Th2 cells induced by helminths have been previously shown to impair immunity to microbial infections [2–5]. We hypothesized, therefore, that the potent Th2 response induced by *H. polygyrus* [27] may be inhibiting effective bacterial clearance, leading to *S.* Typhimurium persistence. To test this, we co-infected mice that are unable to mount a Th2 response. Surprisingly, similar to co-infected wildtype mice, both *il4*-deficient, and *stat6*-deficient co-infected mice failed to clear *S.* Typhimurium from the small intestine by day nine post-infection (Figure 3), suggesting that during co-infection increased susceptibility to secondary bacterial infection is independent of Th2 cells.

In addition to induction of Th2 cells, *H. polygyrus* also stimulates expansion and activation of Tregs [29]. Therefore, Treg mediated immunosuppression of antibacterial responses could account for elevated bacteria burdens in co-infected mice. To test this, we co-infected *rag1*-deficient mice, which lack all mature T cells including Tregs, as well as all mature B cells [30]. We compared *S.* Typhimurium burdens between singly-infected and helminth co-infected *rag1*-deficient mice one day following *S.* Typhimurium infection, before differences in susceptibility to *S.* Typhimurium between wildtype and *rag*1-deficient mice emerge [31]. Similar to wildtype

mice, at one day following *S.* Typhimurium infection, helminth co-infected *rag1*-deficient mice had dramatically elevated *S.* Typhimurium burdens in the small intestine, compared to *rag1*-deficient mice infected with *S.* Typhimurium alone (Figure 4). This suggests that during co-infection suppression of immunity to *S.* Typhimurium is not mediated by helminth-induced Tregs. Together these data demonstrate that helminth infection can impair resistance to bacterial pathogens independently of Th2 or Treg conditioning of host immunity.

Helminth infection alters the metabolic profile of the small intestine

Colonization with helminth parasites has been associated with changes to the intestinal microbiota in both mice and humans [32]. *H. polygyrus* infection causes profound shifts in the composition of the small intestinal microbiota [33–35]. Alterations to the microbiota imposed by *H. polygyrus* have recently been demonstrated to enhance production of microbiota-derived short chain fatty acids, which can alleviate allergic airway inflammation [36]. Helminth infection has also been shown to inhibit the development of inflammatory bowel disease by reducing the prevalence of specific inflammatory species within the microbiota [37]. In both these cases, helminth-induced microbiota changes were seen to target host pathways. We hypothesized there may also be a direct effect of intestinal metabolic changes on concurrent microbial pathogens. We identified metabolites present in the small intestine by ultrahigh-performance liquid chromatography-Fourier transform mass spectrometry (UPLC-FTMS), and assessed the relative abundance of each metabolite between naïve and *H. polygyrus*-infected mice. Helminth infection significantly altered the metabolic profile of the small intestine (Figure 5*A* and *B*, Supplementary Figure 1*A* and *B,* Supplementary Figure 2*A* and *B*). Out of 4593 metabolite features detected, 362 were significantly altered in abundance during *H. polygyrus* infection ($p \leq 0.01$, $\geq$2-fold difference), with 41 upregulated and 321 suppressed during *H. polygyrus* infection (mass-to-

charge ratio [m/z], retention time, and putative identities of metabolite features reported in Supplementary Figure 2*A* and *B*, Supplementary Tables 1 to 4).

Helminth-modulated small intestinal metabolites promote *S.* Typhimurium intracellular invasion

We next aimed to determine whether a helminth-altered metabolome had an impact on the growth or invasive capacity of *S.* Typhimurium. We first tested whether helminth-altered small intestinal metabolites affected the growth rate of *S.* Typhimurium, and found no evidence that helminth-altered small intestinal metabolites promoted the growth of *S.* Typhimurium in an in vitro growth assay (Supplementary Figure 3*A* and *B*). We next investigated whether exposure to helminth-modulated small intestinal metabolites altered the expression levels of *S.* Typhimurium virulence genes. HilA is a bacterial transcription factor that plays a central role in regulating expression of *S.* Typhimurium genes controlling intracellular invasion, which are encoded within *Salmonella* pathogenicity island 1 (SPI-1) [38]. We found that *hilA* expression was inhibited in *S.* Typhimurium cultured with metabolites from naïve mice but not by metabolites from *H. polygyrus*-infected mice (Figure 6*A*). Expression levels of *sipA* and *sprB*, which are also found within the SPI-1 locus, were likewise elevated after culture with small intestinal metabolites from *H. polygyrus*-infected mice compared to after culture with small intestinal metabolites from naïve mice (Figure 6*A*). These data indicate that small intestinal metabolites altered in abundance during helminth infection promote the expression of virulence genes in *S.* Typhimurium. To determine whether the altered expression of *S.* Typhimurium virulence genes after exposure to helminth-modulated metabolites corresponded with an altered invasive capacity of *S.* Typhimurium, we tested the effect of metabolites from naïve or *H. polygyrus*-infected mice on *S.* Typhimurium intracellular invasion. Metabolites extracted from the small intestine of naïve

277 mice, either 129S1/SvImJ or C57BL/6, significantly suppressed the ability of *S.* Typhimurium to
278 invade human epithelial (HeLa) cells (Figure 6*B*). In contrast, metabolites extracted from the
279 small intestine of *H. polygyrus*-infected mice did not suppress the ability of *S.* Typhimurium to
280 invade HeLa cells (Figure 6*B*). These data reveal for the first time that modulation of intestinal
281 metabolites during helminth infection directly affects the invasive capacity of pathogenic *S.*
282 Typhimurium bacteria. Together our data reveal a new interaction in helminth-bacterial co-
283 infection, in which helminth infection disrupts the protective composition of the intestinal
284 metabolome, allowing for increased intracellular invasion and colonization by pathogenic
285 bacteria.

Discussion:

A number of studies have demonstrated that an ongoing helminth infection can result in heightened susceptibility to microbial pathogens. This was attributed to helminth mediated immunomodulation that acted to compromise the development of antimicrobial immune responses [1–5,13]. In this study, we describe a novel mechanism by which helminths increase susceptibility to a microbial pathogen, independently of immune conditioning toward Th2 or Treg responses. We provide evidence to show that the presence of helminths disrupts the metabolic composition of the intestine, and the resultant shift in metabolites directly alters the invasive capacity of the intracellular bacterial pathogen *S.* Typhimurium.

Salmonella invasion gene expression is strongly repressed by metabolites extracted from the feces of naïve mice or humans [39]. These inhibitory metabolites are likely derived from both the microbiota as well as the mammalian host, as metabolites extracted from the feces of both germ-free and conventionally-raised mice inhibited *Salmonella* invasion gene expression, although to a lesser extent by metabolites from germ-free mice [39]. Disruption of the intestinal metabolic environment by antibiotic treatment can promote *S.* Typhimurium expansion in mice [40]. Antibiotic treatment induces host expression of *inducible nitric oxide synthase* (*iNOS*), which mediates elevated carbohydrate oxidation, releasing galactarate and glucarate that can promote the expansion of *S.* Typhimurium [40]. *H. polygyrus* infection could disrupt the intestinal metabolome by shifting the composition of the microbiota, thereby altering the abundance microbiota-derived products [33–35], or by interfering with host metabolism. Additionally, it is possible that metabolites produced directly by helminths [36,41] are responsible for promoting *Salmonella* virulence.

It is becoming increasingly clear that complex communication between kingdoms occurs in the mammalian intestine. The bacterial microbiota and intestinal helminths share a niche within the host, and can influence each other's fitness and persistence [32]. For example, the presence of the microbiota is critical for the establishment of *Trichuris muris*, a murine whipworm whose eggs hatch in the ceca [42]. For hatching, the eggs require direct contact with structural components of microbes within the intestinal microbiota [42]. Specific species within the microbiota can also affect the chronicity of adult helminths. *Lactobacillus* species promote the persistence of adult *H. polygyrus* and *T. muris* worms, likely through the induction of Tregs and inhibition of Th2 responses directed against the parasites [33,43]. A common pathway of inter-bacterial communication in the intestine is through the production of bacterial-derived metabolites, which can shape the population dynamics of the bacterial microbiota, as well as influencing the ability of pathogenic bacteria to colonize the intestine [44]. Our work provides the first example of how helminths can influence the virulence of a pathogenic bacteria through an altered small intestinal metabolome.

A helminth-altered cecal metabolome has been shown to mediate, at least in part, the suppression of airway inflammation during helminth infection in a murine model of allergic asthma [36]. It has been previously demonstrated that helminth infection results in elevated levels of short chain fatty acids (SCFAs) in the ceca of mice, which enhanced the suppressive function of Tregs and protected against airway inflammation [36]. Helminths may have evolved the ability to shift the metabolite profile towards one which promotes their own chronicity, for example, through inducing SCFA which have been shown to induce and enhance the suppressive function of Tregs [45–47]. There is a current interest in the use of helminths, or helminth-derived products, for the therapeutic treatment of inflammatory diseases including allergy and inflammatory bowel

disease [48]. As our data and others suggests that helminth infection can also increase susceptibility to microbial infections [2–6], it will be important to fully characterize the pathways by which helminths affect host physiology, such that susceptibility to pathogenic microbes during therapeutic administration of helminths can be predicted and controlled.

Helminths are potent immunomodulators, which can alter host immunity to infectious and immune-mediated diseases through multiple mechanisms, dependent on the disease context, host genetics, and the microbiota [13,36,37]. Both helminths and the microbiota have potent immunomodulatory effects during inflammatory and infectious diseases [13,32,49,50]. Our data identify a novel mechanism by which a helminth-modified metabolic environment can promote the ability of a bacterial pathogen to colonize the intestine. Understanding the mechanisms by which helminths promote susceptibility to microbial co-infections will aid disease treatment and prevention strategies in the world regions where helminths are prevalent.

Word count: 3500

Funding:

Metabolomics analysis was performed at the UVic-Genome BC Proteomics Centre and was supported by funding to 'The Metabolomics Innovation Centre (TMIC)' through the Genome Innovations Network (GIN) from Genome Canada, Genome Alberta and Genome British Columbia for operations (250MET and 7203) and technology development (215MET and MC3T)'. L.A.R. was supported by Postdoctoral Fellowship awards from the Canadian Institutes of Health Research (CIHR) and the Michael Smith Foundation for Health Research (MSFHR) in partnership with AllerGen. N.G. was supported by Postdoctoral Fellowship awards from CIHR and MSFHR. E.M.B. was supported by a CIHR Doctoral Research Award and a Four Year Doctoral Fellowship (4YF) from UBC. N.C.M was supported by a Vanier Canada Graduate Scholarship and a 4YF from UBC. Y.V. was supported by Postdoctoral Fellowship awards from CIHR and the MSFHR. C.H.B. was supported by the Leading Edge Endowment Fund, the Segal McGill Family Chair in Molecular Oncology at the Jewish General Hospital, Montreal, Quebec, Canada, the Warren Y. Soper Foundation at the Jewish General Hospital, Montreal, Quebec, Canada and the Alvin Segal Family Foundation at the Jewish General Hospital, Montreal, Quebec, Canada. Work in the laboratory of G.P.-W. was supported by CIHR (MOP-126061) and funds from UBC. G.P.-W. is a MSFHR Scholar and holds a CIHR New Investigator Award granted in partnership with the Crohn's and Colitis Foundation Canada, and the Canadian Association of Gastroenterology. Work in the laboratory of B.B.F. was supported by operating grants from CIHR (MOP-133561 and MOP-299601), the Canadian Institute for Advanced Research (CIFAR) and Institut Merieux. B.B.F. is a Peter Wall Distinguished Professor at UBC.

Acknowledgments:

We thank Dr. Kelly McNagny at UBC for provision of *rag1*$^{-/-}$ mice.

References:

1. Salgame P, Yap GS, Gause WC. Effect of helminth-induced immunity on infections with microbial pathogens. Nat Immunol. **2013**; 14(11):1118–26.

2. Chen C-C, Louie S, McCormick B, Walker WA, Shi HN. Concurrent infection with an intestinal helminth parasite impairs host resistance to enteric Citrobacter rodentium and enhances Citrobacter-induced colitis in mice. Infect Immun. **2005**; 73(9):5468–81.

3. Osborne LC, Monticelli LA, Nice TJ, et al. Coinfection. Virus-helminth coinfection reveals a microbiota-independent mechanism of immunomodulation. Science. **2014**; 345(6196):578–82.

4. Reese TA, Wakeman BS, Choi HS, et al. Helminth infection reactivates latent γ-herpesvirus via cytokine competition at a viral promoter. Science. **2014**; 345(6196):573–7.

5. Hsieh Y-J, Fu C-L, Hsieh MH. Helminth-induced interleukin-4 abrogates invariant natural killer T cell activation-associated clearance of bacterial infection. Infect Immun. **2014**; 82(5):2087–97.

6. Su L, Su C, Qi Y, et al. Coinfection with an intestinal helminth impairs host innate immunity against Salmonella enterica serovar Typhimurium and exacerbates intestinal inflammation in mice. Infect Immun. **2014**; 82(9):3855–66.

7. Harris JB, Podolsky MJ, Bhuiyan TR, et al. Immunologic responses to Vibrio cholerae in patients co-infected with intestinal parasites in Bangladesh. PLoS Negl Trop Dis. **2009**; 3(3):e403.

8. Elias D, Mengistu G, Akuffo H, Britton S. Are intestinal helminths risk factors for developing active tuberculosis? Trop Med Int Health. **2006**; 11(4):551–8.

9. Resende Co T, Hirsch CS, Toossi Z, Dietze R, Ribeiro-Rodrigues R. Intestinal helminth co-infection has a negative impact on both anti-Mycobacterium tuberculosis immunity and clinical response to tuberculosis therapy. Clin Exp Immunol. **2007**; 147(1):45–52.

10. Downs JA, Mguta C, Kaatano GM, et al. Urogenital schistosomiasis in women of reproductive age in Tanzania's Lake Victoria region. Am J Trop Med Hyg. **2011**; 84(3):364–9.

11. Hesran J-Y Le, Akiana J, Ndiaye EHM, Dia M, Senghor P, Konate L. Severe malaria attack is associated with high prevalence of Ascaris lumbricoides infection among children in rural Senegal. Trans R Soc Trop Med Hyg. **2004**; 98(7):397–9.

12. Degarege A, Legesse M, Medhin G, Animut A, Erko B. Malaria and related outcomes in patients with intestinal helminths: a cross-sectional study. BMC Infect Dis. **2012**; 12:291.

13. Maizels RM, Yazdanbakhsh M. Immune regulation by helminth parasites: cellular and molecular mechanisms. Nat Rev Immunol. **2003**; 3(9):733–44.

14. Haeryfar SMM, DiPaolo RJ, Tscharke DC, Bennink JR, Yewdell JW. Regulatory T cells suppress CD8+ T cell responses induced by direct priming and cross-priming and moderate immunodominance disparities. J Immunol. **2005**; 174(6):3344–51.

15. Johanns TM, Ertelt JM, Rowe JH, Way SS. Regulatory T cell suppressive potency dictates the balance between bacterial proliferation and clearance during persistent Salmonella infection. PLoS Pathog. **2010**; 6(8):e1001043.

16. Marple A, Wu W, Shah S, et al. Cutting Edge: Helminth Coinfection Blocks Effector Differentiation of CD8 T Cells through Alternate Host Th2- and IL-10–Mediated Responses. J Immunol. **2016**; 198(2):1601741.

17. Perona-Wright G, Mohrs K, Mohrs M. Sustained signaling by canonical helper T cell cytokines throughout the reactive lymph node. Nat Immunol. **2010**; 11(6):520–6.

18. Li Y, Chen H-L, Bannick N, et al. Intestinal helminths regulate lethal acute graft-versus-host disease and preserve the graft-versus-tumor effect in mice. J Immunol. **2015**; 194(3):1011–20.

19. Wilson MS, Taylor MD, Balic A, Finney CAM, Lamb JR, Maizels RM. Suppression of allergic airway inflammation by helminth-induced regulatory T cells. J Exp Med. **2005**; 202(9):1199–212.

20. Kitagaki K, Businga TR, Racila D, Elliott DE, Weinstock J V, Kline JN. Intestinal helminths protect in a murine model of asthma. J Immunol. **2006**; 177(3):1628–35.

21. Mohrs M, Shinkai K, Mohrs K, Locksley RM. Analysis of Type 2 Immunity In Vivo with a Bicistronic IL-4 Reporter. Immunity. **2001**; 15(2):303–311.

22. Mohrs K, Wakil AE, Killeen N, Locksley RM, Mohrs M. A two-step process for cytokine production revealed by IL-4 dual-reporter mice. Immunity. **2005**; 23(4):419–29.

23. Kaplan MH, Schindler U, Smiley ST, Grusby MJ. Stat6 is required for mediating responses to IL-4 and for development of Th2 cells. Immunity. **1996**; 4(3):313–9.

24. Hoiseth SK, Stocker BAD. Aromatic-dependent Salmonella typhimurium are non-virulent and effective as live vaccines. Nature. **1981**; 291(5812):238–239.

25. Xia J, Sinelnikov I V., Han B, Wishart DS. MetaboAnalyst 3.0--making metabolomics more meaningful. Nucleic Acids Res. **2015**; 43(W1):W251-7.

26. Xia J, Psychogios N, Young N, Wishart DS. MetaboAnalyst: a web server for metabolomic data analysis and interpretation. Nucleic Acids Res. **2009**; 37(Web Server

issue):W652-60.

27. Reynolds LA, Filbey KJ, Maizels RM. Immunity to the model intestinal helminth parasite Heligmosomoides polygyrus. Semin. Immunopathol. 2012. p. 829–846.

28. Govoni G, Vidal S, Gauthier S, Skamene E, Malo D, Gros P. The Bcg/Ity/Lsh locus: genetic transfer of resistance to infections in C57BL/6J mice transgenic for the Nramp1 Gly169 allele. Infect Immun. **1996**; 64(8):2923–9.

29. Grainger JR, Smith KA, Hewitson JP, et al. Helminth secretions induce de novo T cell Foxp3 expression and regulatory function through the TGF-β pathway. J Exp Med. **2010**; 207(11):2331–41.

30. Mombaerts P, Iacomini J, Johnson RS, Herrup K, Tonegawa S, Papaioannou VE. RAG-1-deficient mice have no mature B and T lymphocytes. Cell. **1992**; 68(5):869–77.

31. Kupz A, Bedoui S, Strugnell RA. Cellular requirements for systemic control of Salmonella enterica serovar Typhimurium infections in mice. Infect Immun. **2014**; 82(12):4997–5004.

32. Reynolds LA, Finlay BB, Maizels RM. Cohabitation in the Intestine: Interactions among Helminth Parasites, Bacterial Microbiota, and Host Immunity. J Immunol. **2015**; 195(9):4059–66.

33. Reynolds LA, Smith KA, Filbey KJ, et al. Commensal-pathogen interactions in the intestinal tract: lactobacilli promote infection with, and are promoted by, helminth parasites. Gut Microbes. **2014**; 5(4):522–32.

34. Walk ST, Blum AM, Ewing SA-S, Weinstock J V, Young VB. Alteration of the murine gut microbiota during infection with the parasitic helminth Heligmosomoides polygyrus.

Inflamm Bowel Dis. **2010**; 16(11):1841–9.

35. Rausch S, Held J, Fischer A, et al. Small intestinal nematode infection of mice is associated with increased enterobacterial loads alongside the intestinal tract. PLoS One. **2013**; 8(9):e74026.

36. Zaiss MM, Rapin A, Lebon L, et al. The Intestinal Microbiota Contributes to the Ability of Helminths to Modulate Allergic Inflammation. Immunity. **2015**; 43(5):998–1010.

37. Ramanan D, Bowcutt R, Lee SC, et al. Helminth infection promotes colonization resistance via type 2 immunity. Science. **2016**; 352(6285):608–12.

38. Bajaj V, Lucas RL, Hwang C, Lee CA. Co-ordinate regulation of Salmonella typhimurium invasion genes by environmental and regulatory factors is mediated by control of hilA expression. Mol Microbiol. **1996**; 22(4):703–14.

39. Antunes LCM, McDonald JAK, Schroeter K, et al. Antivirulence activity of the human gut metabolome. MBio. **2014**; 5(4):e01183-14.

40. Faber F, Tran L, Byndloss MX, et al. Host-mediated sugar oxidation promotes post-antibiotic pathogen expansion. Nature. **2016**; 534(7609):697–9.

41. Tielens AGM, Grinsven KWA van, Henze K, Hellemond JJ van, Martin W. Acetate formation in the energy metabolism of parasitic helminths and protists. Int J Parasitol. **2010**; 40(4):387–97.

42. Hayes KS, Bancroft AJ, Goldrick M, Portsmouth C, Roberts IS, Grencis RK. Exploitation of the intestinal microflora by the parasitic nematode Trichuris muris. Science. **2010**; 328(5984):1391–4.

43. Dea-Ayuela MA, Rama-Iñiguez S, Bolás-Fernandez F. Enhanced susceptibility to

Trichuris muris infection of B10Br mice treated with the probiotic Lactobacillus casei. Int Immunopharmacol. **2008**; 8(1):28–35.

44. Vogt SL, Peña-Díaz J, Finlay BB. Chemical communication in the gut: Effects of microbiota-generated metabolites on gastrointestinal bacterial pathogens. Anaerobe. **2015**; 34:106–15.

45. Arpaia N, Campbell C, Fan X, et al. Metabolites produced by commensal bacteria promote peripheral regulatory T-cell generation. Nature. **2013**; 504(7480):451–5.

46. Smith PM, Howitt MR, Panikov N, et al. The microbial metabolites, short-chain fatty acids, regulate colonic Treg cell homeostasis. Science. **2013**; 341(6145):569–73.

47. Furusawa Y, Obata Y, Fukuda S, et al. Commensal microbe-derived butyrate induces the differentiation of colonic regulatory T cells. Nature. **2013**; 504(7480):446–50.

48. Fleming JO, Weinstock J V. Clinical trials of helminth therapy in autoimmune diseases: rationale and findings. Parasite Immunol. **2015**; 37(6):277–92.

49. McSorley HJ, Maizels RM. Helminth infections and host immune regulation. Clin Microbiol Rev. **2012**; 25(4):585–608.

50. Belkaid Y, Hand TW. Role of the microbiota in immunity and inflammation. Cell. **2014**; 157(1):121–41.

Figure Legends:

Figure 1. Helminth co-infected 129S1/SvlmJ mice exhibit elevated *S.* Typhimurium burdens in the small intestine. ***A***, Experimental set up. 129S1/SvImJ mice were left naïve or infected with *H. polygyrus* (*Hp*). Fourteen days later, all mice were orally infected with *S.* Typhimurium (*S*T). Nine days later, *S.* Typhimurium cfu counts were determined. ***B***, *S.* Typhimurium cfu counts in the duodenum and jejunum. ***C****, S.* Typhimurium cfu counts in the cecum and colon. ***D***, *S.* Typhimurium cfu counts in the spleen and liver. Data shown are pooled from two independent experiments and are representative of the results from three independent experiments.

Figure 2. Helminth co-infected C57BL/6 mice exhibit elevated *S.* Typhimurium burdens in the small intestine. ***A***, Experimental set up. C57BL/6 mice were left naïve or infected with *H. polygyrus* (*Hp*). Fourteen days later, all mice were orally infected with *aroA* mutant *S.* Typhimurium (*S*T). One and nine day(s) later, *S.* Typhimurium cfu counts were determined. ***B***, *S.* Typhimurium cfu counts in the duodenum and jejunum. ***C****, S.* Typhimurium cfu counts in the cecum and colon. ***D***, *S.* Typhimurium cfu counts in the spleen and liver. Data shown are pooled from two independent experiments and are representative of the results from four independent experiments.

Figure 3. Elevated *S.* Typhimurium burdens in helminth co-infected mice are independent of induction of Th2 cells.

C57BL/6, *il4*$^{-/-}$ and *stat6*$^{-/-}$ mice were left naïve or infected with *H. polygyrus.* Fourteen days later, all mice were orally infected with *aroA* mutant *S.* Typhimurium. Nine days later, *S.* Typhimurium cfu counts were determined in the duodenum and jejunum. Data shown are pooled from two independent experiments.

Figure 4. Elevated *S.* Typhimurium burdens in helminth co-infected mice are independent of induction of Treg cells.

C57BL/6 and *rag1*$^{-/-}$ mice were left naïve or infected with *H. polygyrus.* Fourteen days later, all mice were orally infected with *aroA* mutant *S.* Typhimurium. One day later, *S.* Typhimurium cfu counts were determined in the duodenum and jejunum. Data shown are pooled from three independent experiments.

Figure 5. Helminth infection alters the metabolic profile of the small intestine.

A, The differential abundance of small intestinal metabolites from naïve or day-14 *H. polygyrus*-infected (*Hp*) 129S1/SvImJ mice was determined by UPLC-FTMS. A principal component analysis (PCA) plot was generated from metabolites detected in positive ion mode. ***B***, A heat map showing the relative abundance of all metabolites detected in naïve and day-14 *H. polygyrus*–infected mice 129S1/SvImJ mice, detected in positive ion mode. Clustering of naïve and *H. polygyrus*-infected mice is shown using a Euclidean distance and Ward clustering algorithm.

Figure 6. Helminth-modified small intestinal metabolites promote intracellular invasion by *S.* Typhimurium. ***A***, *aroA* mutant *S.* Typhimurium bacteria were cultured without metabolites (control) or with metabolites extracted from the small intestine of naïve or *H. polygyrus*-infected C57BL/6 mice. Expression levels of *S.* Typhimurium *hilA*, *sipA* and *sprB* were then determined. Each data point represents gene expression levels of three *S.* Typhimurium cultures that were split and cultured with metabolites from each group. Data shown are representative of results from four independent experiments that each used independent mice and *S.* Typhimurium cultures. ***B***, Wildtype or aroA mutant *S.* Typhimurium bacteria were cultured without metabolites (control) or with metabolites extracted from the small intestine of naïve or *H. polygyrus*-infected 129S1/SvImJ or C57BL/6 mice, prior to infection of HeLa cells. Each data point represents a technical replicate of HeLa cells infected with *S.* Typhimurium that had been cultured with metabolites pooled from 3-5 naïve or 3 *H. polygyrus*-infected mice. Data are representative of results from two (129S1/SvImJ) or three (C57BL/6) independent experiments that each used independent mice and *S.* Typhimurium cultures.

Footnote Page:

1) The authors declare that no conflicts of interest exist.
2) Work in the laboratory of G.P.-W. was supported by CIHR (MOP-126061) and funds from UBC. G.P.-W. is a MSFHR Scholar and holds a CIHR New Investigator Award granted in partnership with the Crohn's and Colitis Foundation Canada, and the Canadian Association of Gastroenterology. Work in the laboratory of B.B.F. was supported by operating grants from CIHR (MOP-133561 and MOP-299601), the Canadian Institute for Advanced Research (CIFAR) and Institut Merieux.
3) Data from this manuscript has been presented by L.A.R. as an oral presentation at the Mucosal Immunology Symposium 'Microbiota and Mucosal Immunity: Rules of Engagement in Health and Disease' in Toronto, Canada, July 2016 (Abstract #OR.38).
4) Correspondence to:

Name: B. Brett Finlay. **Address:** #301 – 2185 East Mall, Michael Smith Laboratories, University of British Columbia, Vancouver, BC, V6T 1Z4, Canada. **Telephone:** (+1) 604-822-2210. **e-mail:** bfinlay@msl.ubc.ca.

Or, to:

Name: Georgia Perona-Wright. **Address:** Institute of Infection Immunity and Inflammation, University of Glasgow, Sir Graeme Davies Building, 120 University Place, Glasgow, G12 8TA, United Kingdom. **Telephone:** (+44) 141-330-5844. **e-mail:** georgia.perona-wright@glasgow.ac.uk
5) Current address for Lisa A. Reynolds: Department of Biochemistry and Microbiology, University of Victoria, Victoria, BC, V8P 5C2, Canada.

Current address for Stephen A. Redpath: Deeley Research Centre, British Columbia Cancer Agency, Victoria, BC, V8R 6V5, Canada.

Current address for Georgia Perona-Wright: Institute of Infection Immunity and Inflammation, University of Glasgow, Glasgow, G12 8TA, United Kingdom.

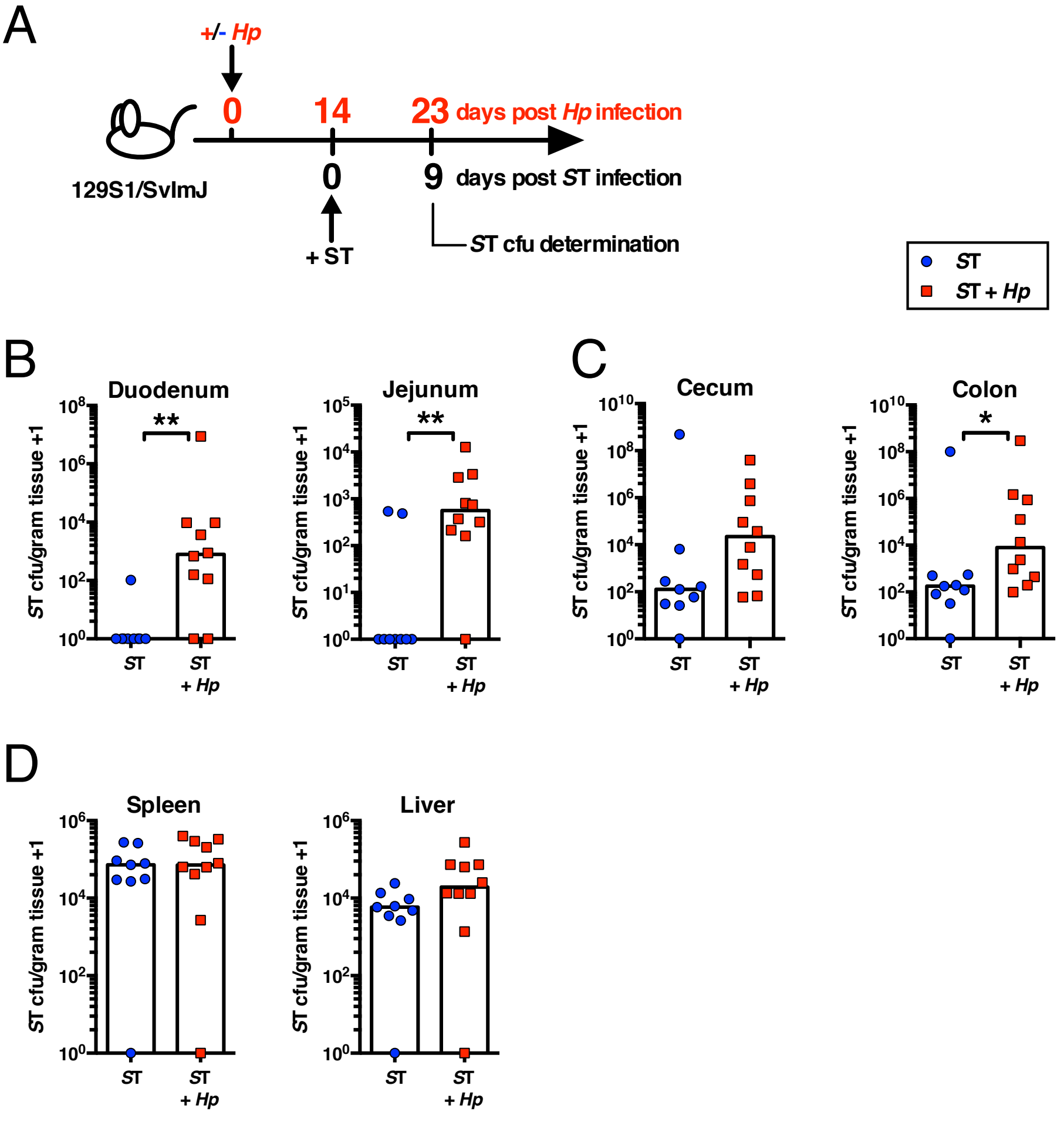
A
+/- Hp
0
14
23 days post Hp infection
129S1/SvImJ
0
9 days post ST infection
+ ST
ST cfu determination
ST
ST + Hp
B
Duodenum
Jejunum
C
Cecum
Colon
D
Spleen
Liver
ST cfu/gram tissue +1
**
*

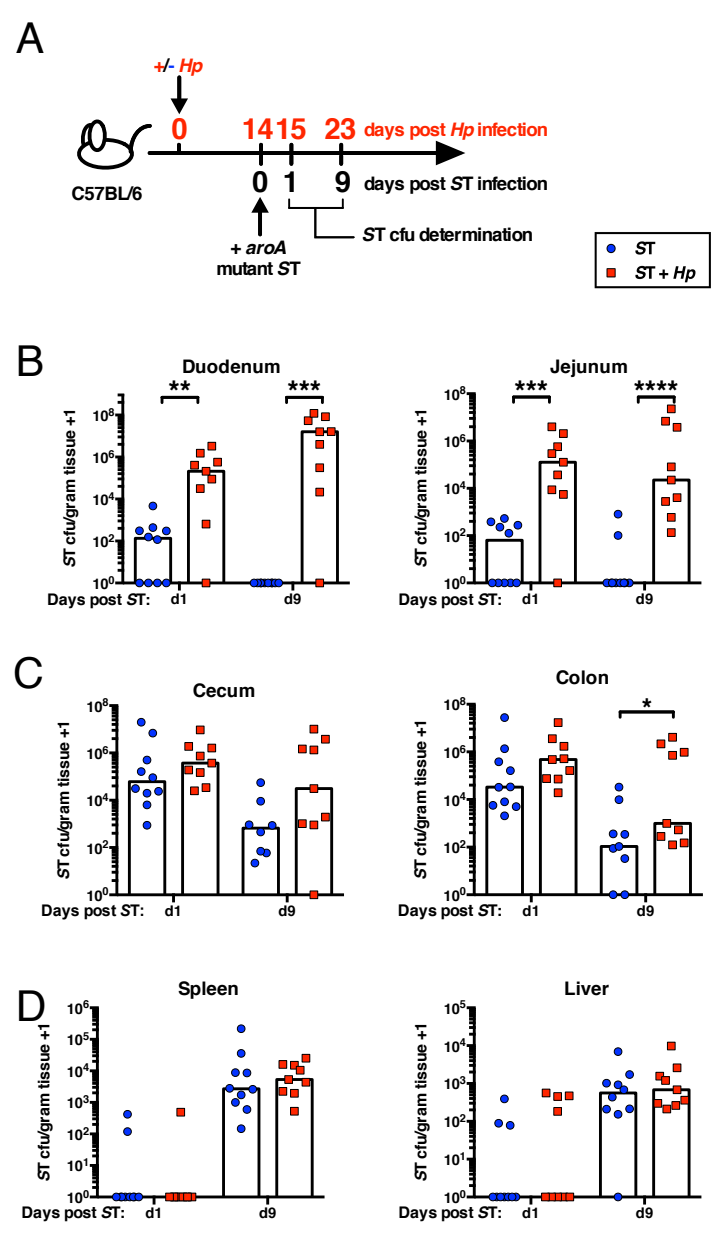
A
+/- Hp
0
14
15
23
days post Hp infection
C57BL/6
0
1
9
days post ST infection
+ aroA mutant ST
ST cfu determination
ST
ST + Hp
B
Duodenum
Jejunum
ST cfu/gram tissue +1
Days post ST:
d1
d9
C
Cecum
Colon
D
Spleen
Liver

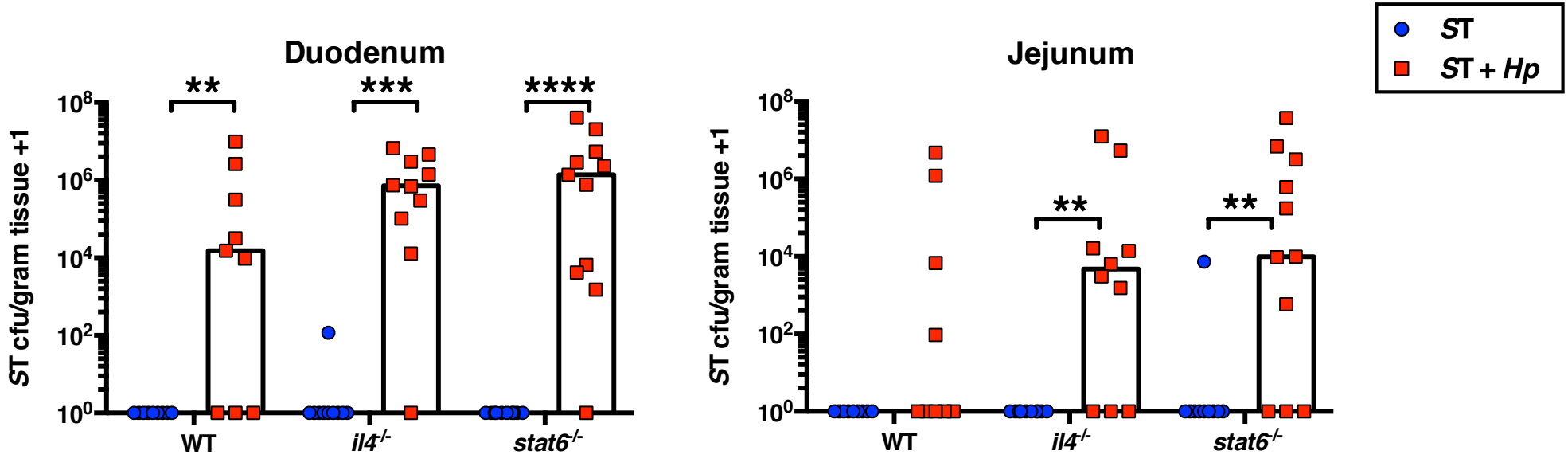
Duodenum
Jejunum
ST
ST + Hp
ST cfu/gram tissue +1
10^8
10^6
10^4
10^2
10^0
**
***
****
**
**
WT
il4-/-
stat6-/-

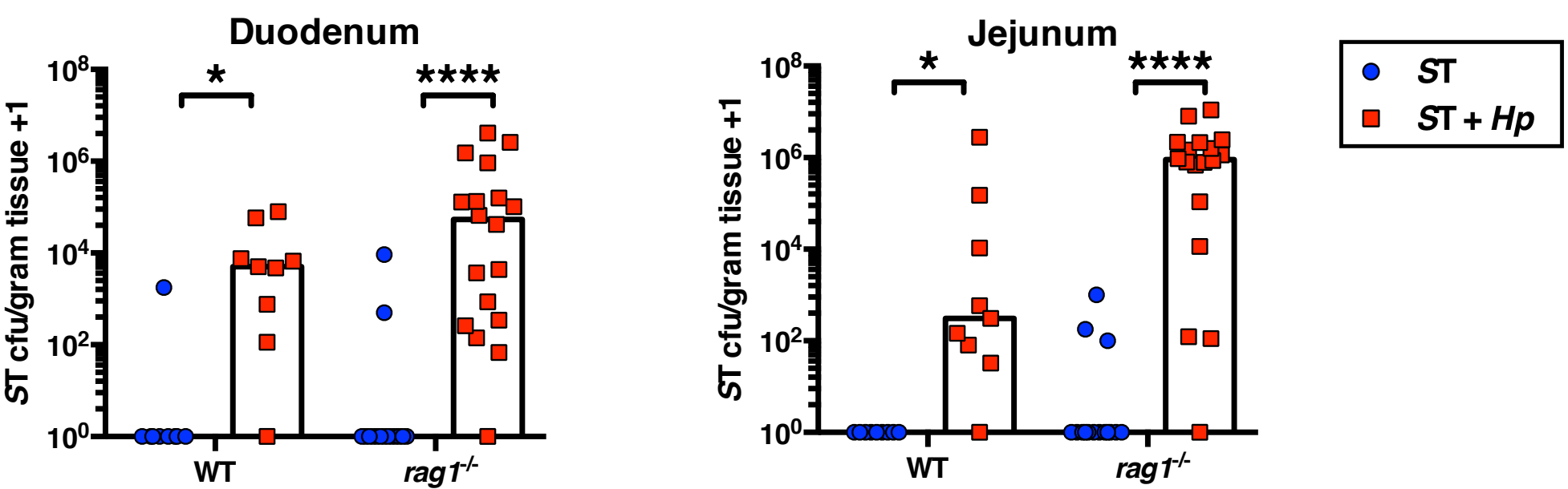
Duodenum
Jejunum
ST cfu/gram tissue +1
10^8
10^6
10^4
10^2
10^0
*
****
WT
rag1-/-
ST
ST + Hp

A

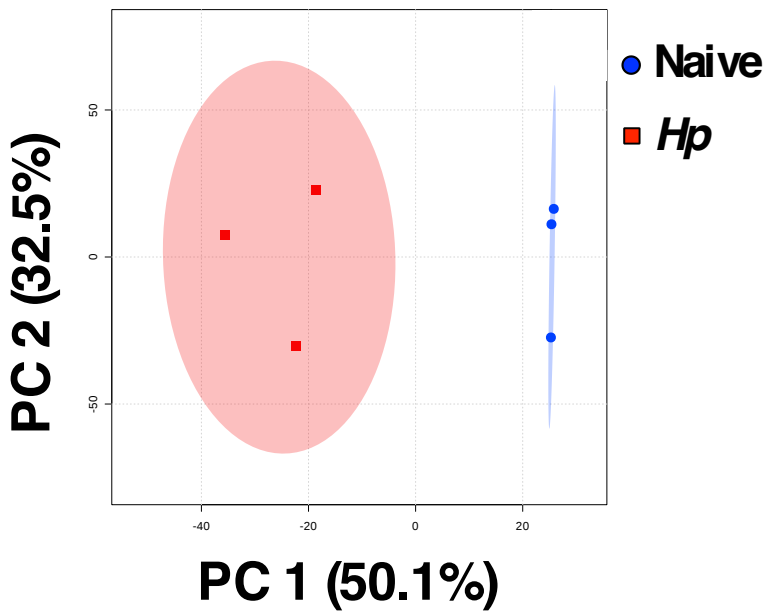
Naive
Hp
PC 2 (32.5%)
PC 1 (50.1%)
50
0
-50
-40
-20
0
20

B

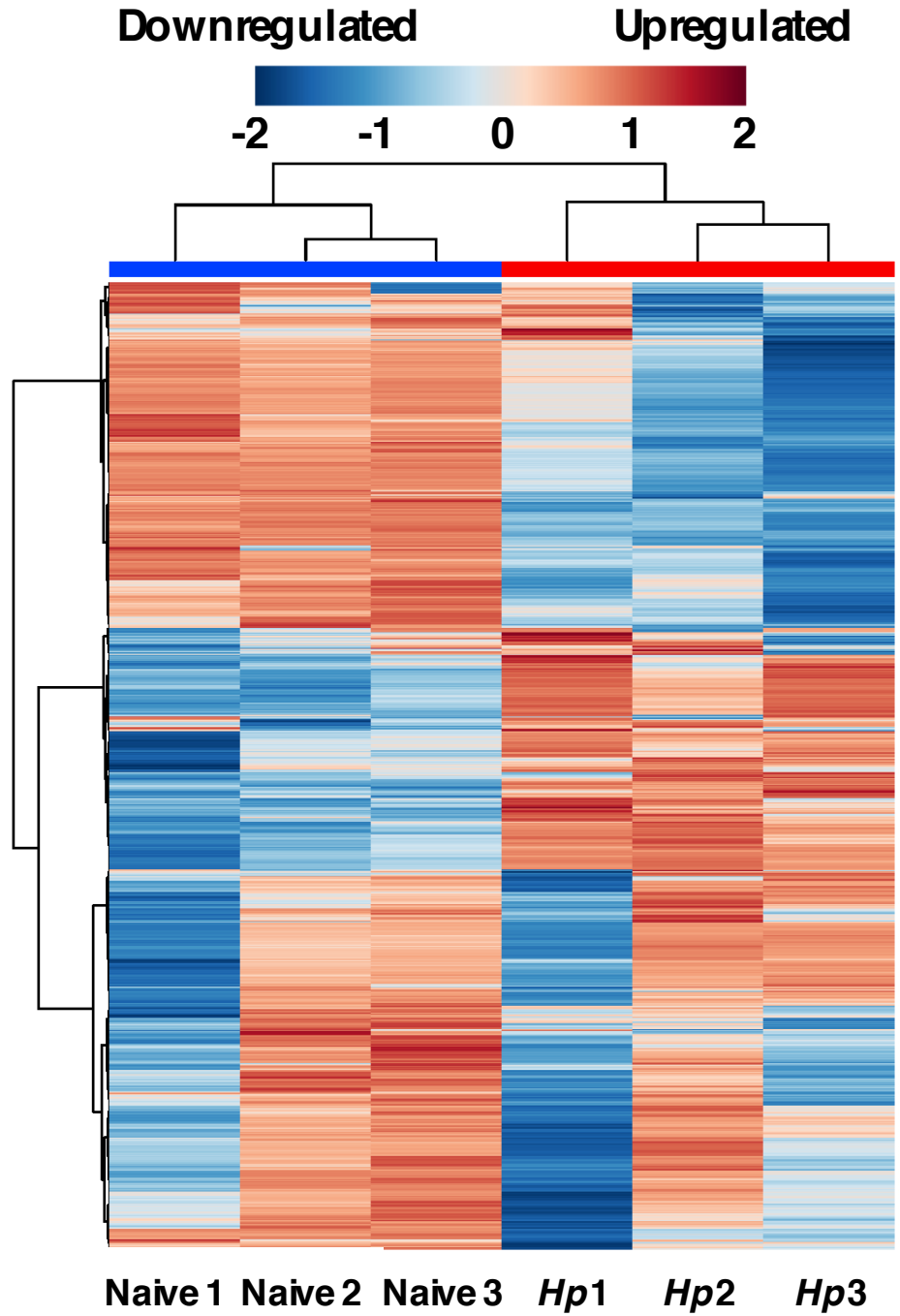
Downregulated
Upregulated
-2
-1
0
1
2
Naive 1
Naive 2
Naive 3
Hp1
Hp2
Hp3

A

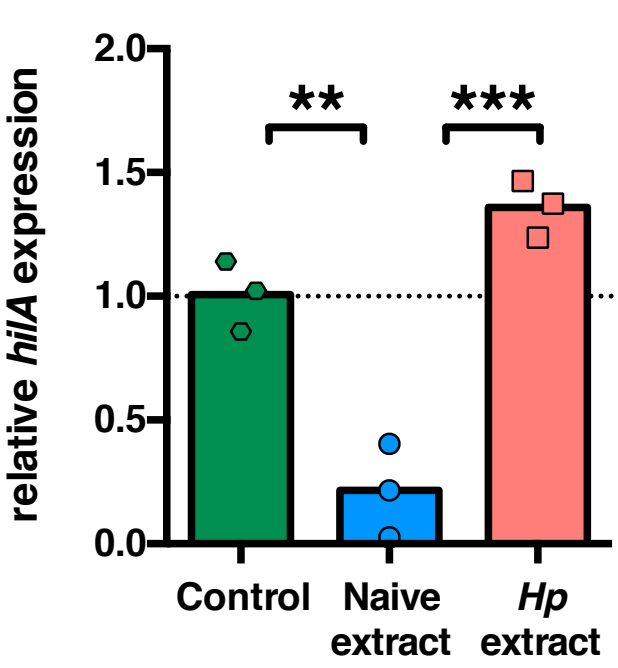
relative *hilA* expression
2.0
1.5
1.0
0.5
0.0
**
***
Control
Naive extract
Hp extract

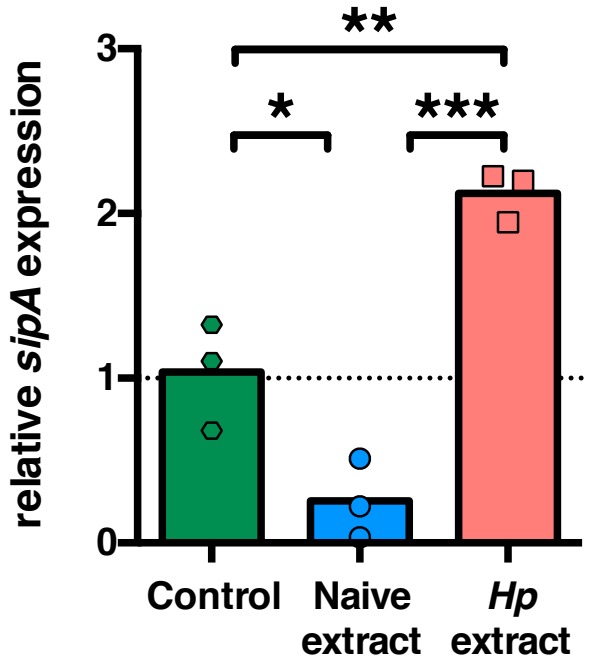
relative *sipA* expression
3
2
1
0
**
*
***
Control
Naive extract
Hp extract

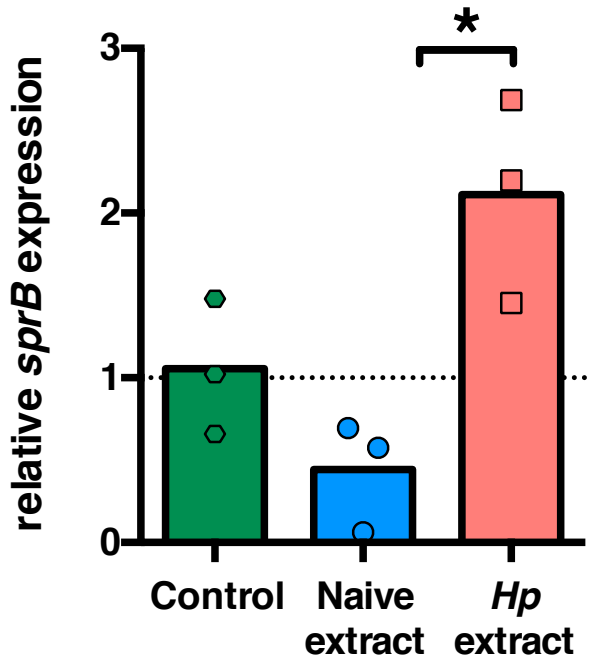
relative *sprB* expression
3
2
1
0
*
Control
Naive extract
Hp extract

B

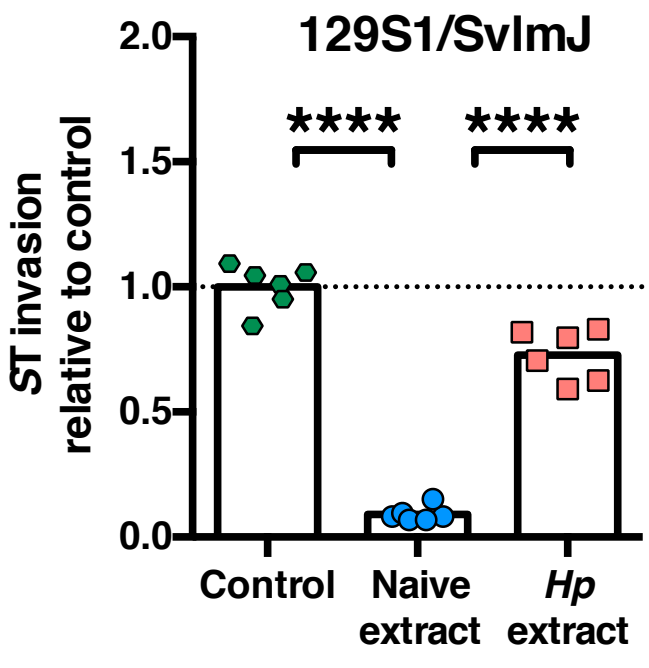
129S1/SvImJ
ST invasion relative to control
2.0
1.5
1.0
0.5
0.0
****
****
Control
Naive extract
Hp extract

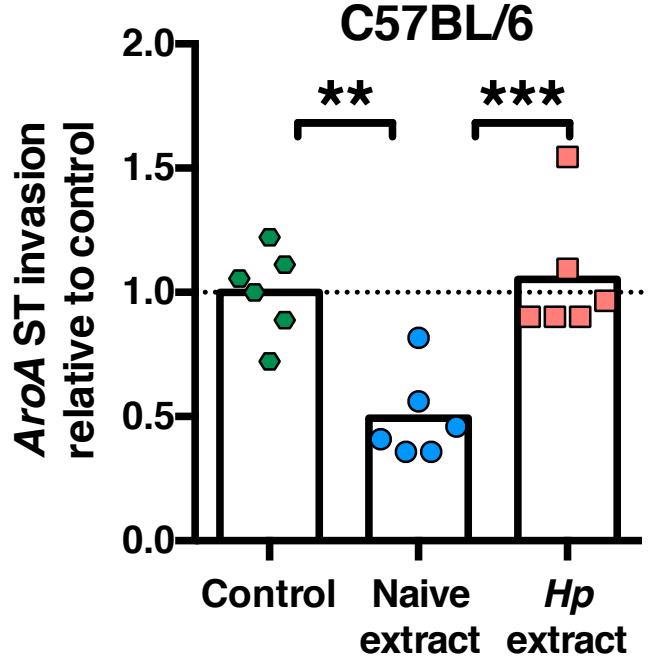
C57BL/6
AroA ST invasion relative to control
2.0
1.5
1.0
0.5
0.0
**
***
Control
Naive extract
Hp extract

Supplementary Methods

Metabolite analysis

Three samples containing metabolite extracts from 25 mg of small intestinal contents from naïve 129S1/SvImJ mice and 3 samples containing extracts from 25 mg of day 14 *H. polygyrus*-infected 129S1/SvImJ mice were obtained as described above. Each sample contained pooled small intestinal content from 2-3 naïve or *H. polygyrus*-infected mice. Samples were sent to the University of Victoria-Genome BC Proteomics Centre for untargeted metabolomics by Ultrahigh-Performance Liquid Chromatography-Fourier transform mass spectrometry (UPLC-FTMS) analysis. Each of the dried residues of intestinal contents was dissolved in 200 µL of 75 % aqueous methanol. After vortex mixing, sonication for 1 minute in an ice water bath, and centrifugation at 15,000 rpm and 5 °C in an Eppendorf 5420 R centrifuge for 10 minutes, 5 µL of the supernatants were injected for UPLC-FTMS into a C8 column (2.1 x 50 mm, 1.7 µm). The UPLC-MS instrument was a Waters Acquity UPLC system coupled to a Thermo Scientific LTQ-Orbitrap Fusion mass spectrometer. The MS instrument was operated in the survey scan mode with Fourier transform (FT) MS detection at a resolution of 120,000 FWHM (m/z 400) for metabolite detection and relative quantitation. For assistance of metabolite identification, LC-MS/MS data using collision induced dissociation were acquired. The metabolites were detected within m/z 80 to 1200 and in positive and negative ion detection modes, respectively. Two LC-MS runs per sample were performed. The mobile phase was 0.01 % formic acid in water (A) and acetonitrile-isopropanol (1:1, v/v) containing 0.01 % formic acid (B) for binary solvent gradient elution. The gradient was 5% to 40 % B in 5 minutes; 40 % to 100 % B in 15 minutes; 100 % B for 2 minutes and then the column was reconditioned at 5 % B for 4 minutes between injections. The flow rate was 0.35 mL/minute and the column temperature was 45 °C.

The positive ion and negative ion UPLC-FTMS datasets were respectively processed using the XCMS (https://xcmsonline.scripps.edu/) suite in R for peak detection, retention time shift correction, peak grouping and peak alignment [1]. Mass de-isotoping was performed manually. The output of the data processing was the retention time, mass to charge ratio (m/z) and peak area of each detected metabolite or metabolite feature from each LC-MS dataset. Welch t-test with unequal variances was applied for the statistical analysis. Multivariate and clustering analyses were carried out using Metaboanalyst version 3.0 software (http://www.metaboanalyst.ca/faces/home.xhtml) [2,3], using a m/z tolerance of 0.0005 and a retention time tolerance of 30 seconds. Data were log transformed and autoscaled. Principal component analysis (PCA) was performed and plots were generated showing separation of data based on the first two principal components. Heat maps were generated showing the relative abundance of all small intestinal metabolites. Maximum abundance was reported in red and minimum abundance was reported in blue. Clustering of samples from different mice was shown using a Euclidean distance and Ward clustering algorithm. Where possible, putative identities of identified metabolite features were assigned using the online Metlin database (https://metlin.scripps.edu/metabo_batch.php) based on the m/z value of each metabolite feature. Statistical analyses were performed separately on datasets from positive and negative ion detection datasets.

In vitro *S.* Typhimurium growth assay

Metabolites extracted from small intestinal contents of naïve C57BL/6 or 129S1/SvImJ mice, or metabolites extracted from small intestinal contents of day 14 *H. polygyrus*-infected C57BL/6 or 129S1/SvImJ mice were resuspended in LB media, and sterile-filtered through a 0.22 μM pore filter unit (Sigma-Aldrich). 150 μl of LB media containing metabolites extracted from 3.75 mg

of small intestinal contents was added to each well of a 96-well transparent flat bottom plate. 4 µl of stationary-phase overnight cultures of *S.* Typhimurium or *aroA* mutant *S.* Typhimurium (as indicated) grown in LB were diluted into LB containing metabolites from naïve or *H. polygyrus*-infected mice, and were shaken at 37 °C for 16 hours in an Infinite® 200 PRO plate reader (Tecan). Absorbance of cultures was measured at 600 nm over 16 hours. Each curve plotted tracks the growth of a S. Typhimurium culture with metabolites extracted from an individual mouse, and error bars denote the standard error of three technical replicates.

Supplemental References

1. Tautenhahn R, Patti GJ, Rinehart D, Siuzdak G. XCMS Online: a web-based platform to process untargeted metabolomic data. Anal Chem. **2012**; 84(11):5035–9.
2. Xia J, Sinelnikov I V., Han B, Wishart DS. MetaboAnalyst 3.0--making metabolomics more meaningful. Nucleic Acids Res. **2015**; 43(W1):W251-7.
3. Xia J, Psychogios N, Young N, Wishart DS. MetaboAnalyst: a web server for metabolomic data analysis and interpretation. Nucleic Acids Res. **2009**; 37(Web Server issue):W652-60.

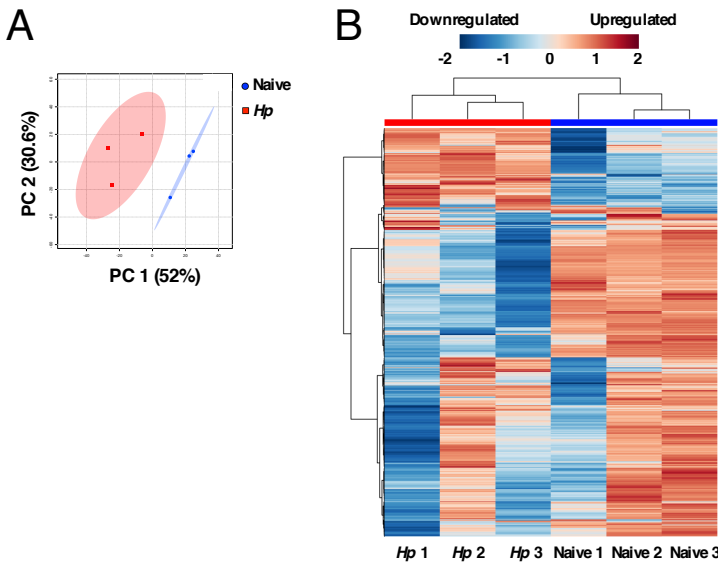

65

66 **Supplementary Figure 1. Helminth infection alters the metabolite profile of the small**
67 **intestine.** ***A***, Untargeted UPLC-FTMS was performed to determine the differential abundance of
68 metabolites in the small intestine of naïve or day 14 *H. polygyrus*-infected (*Hp*) 129S1/SvImJ
69 mice. A principal component analysis (PCA) plot was generated from metabolites detected in the
70 negative ion mode. ***B,*** A heat map showing the relative abundance of all small intestinal
71 metabolites detected in naïve and day 14 *H. polygyrus*–infected mice 129S1/SvImJ mice,
72 detected by in the negative ion mode. Clustering of naïve and day 14 *H. polygyrus*-infected mice
73 is shown using a Euclidean distance and Ward clustering algorithm.

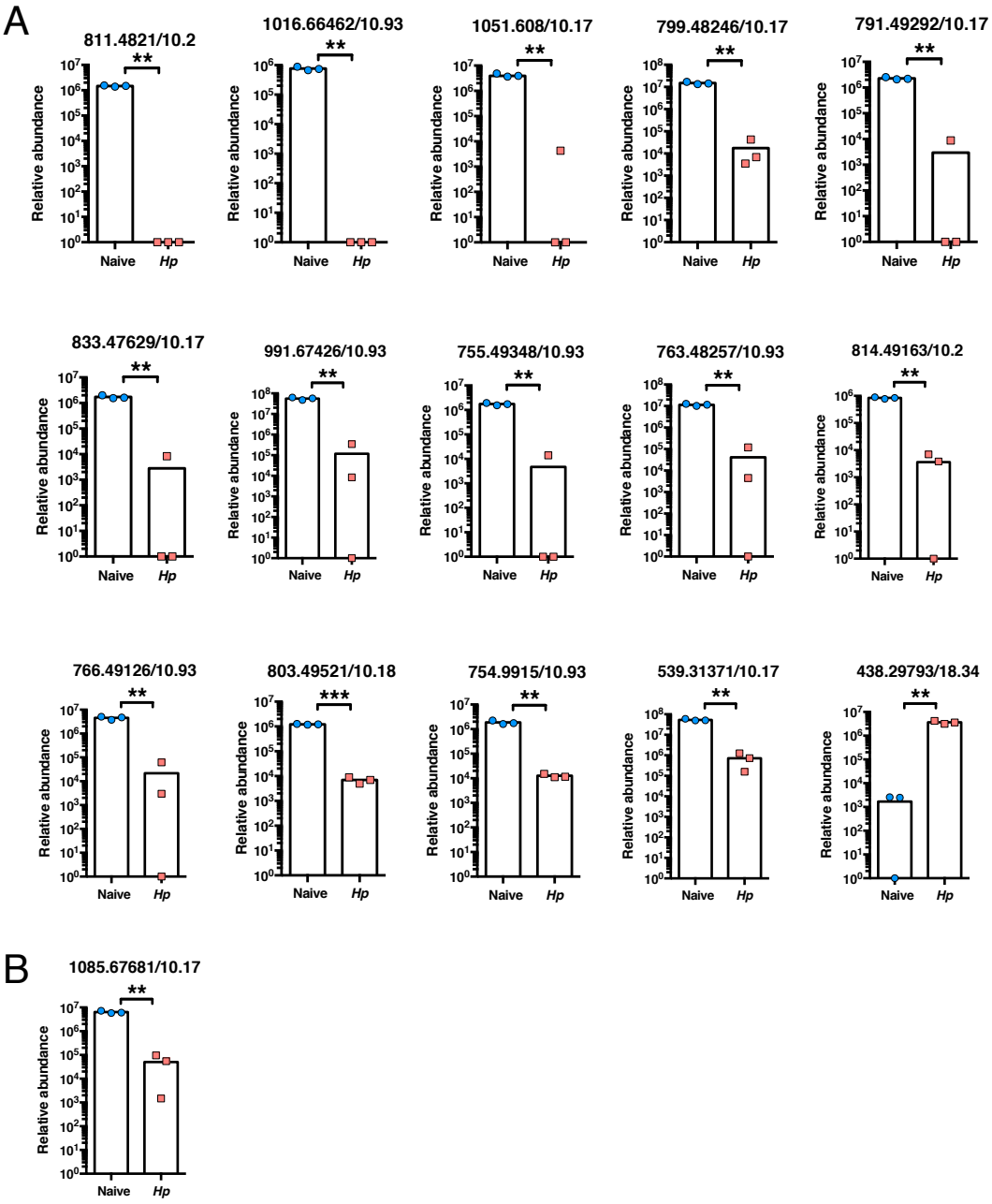

74

75 **Supplementary Figure 2. Helminth infection alters the metabolite profile of the small**
76 **intestine.** Untargeted UPLC-FTMS was performed to identify the differential abundance of
77 metabolites in the small intestine of naïve or day 14 *H. polygyrus*-infected (*Hp*) 129S1/SvImJ
78 mice. The relative abundance of all metabolite features, described by mass to charge ratio (m/z)
79 and retention time (rt) (shown on labels as m/z/rt) is shown. All metabolite features significantly

altered ($p < 0.01$), with greater than a 100-fold difference in abundance between naïve and *H. polygyrus*-infected mice are shown. ***A*****,** Detected in positive ion mode. ***B***, Detected in negative ion mode.

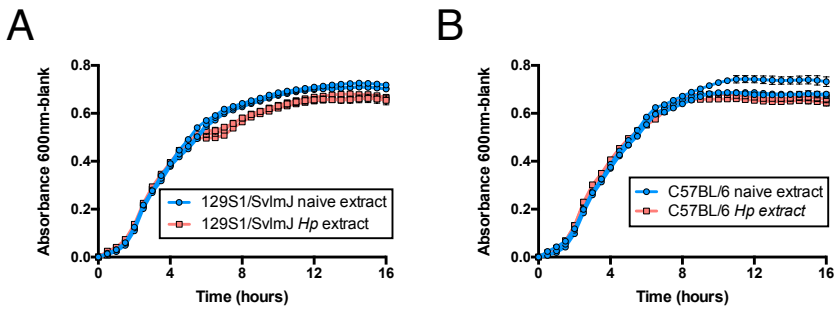

Supplementary Figure 3. Metabolites extracted from the small intestine of *Hp*-infected mice do not increase the growth rate of *S.* Typhimurium. Metabolites were extracted from the small intestine of naïve or day-14 *H.* polygyrus (*Hp*) infected 129S1/SvImJ (***A***) or C57BL/6 (***B***) mice and cultured with wildtype (***A***) or aroA mutant (***B***) *S.* Typhimurium bacteria in LB medium. *S.* Typhimurium growth was tracked over 16 hours by measuring optical density at 600 nm. Each curve tracks the growth of a *S.* Typhimurium culture with metabolites extracted from an individual mouse, and error bars denote the standard error of three technical replicates.

Supplementary Table 1. Putative identities of metabolites detected in positive ion mode upregulated in the small intestine of uninfected mice compared with *H. polygyrus*-infected mice.

Untargeted UPLC-FTMS was performed to identify the differential abundance of metabolites in the small intestine of naïve or day 14 *H. polygyrus*-infected 129S1/SvImJ mice. Those metabolites significantly upregulated (p= <0.01) in the small intestine of naïve, compared to *H. polygyrus*-infected mice, that were detected in positive ion mode, are reported. m/z= mass to charge ratio, rt= column retention time, fold= fold change. Putative identities (IDs) were assigned to each metabolite feature where possible.

m/z	rt	fold	Putative ID (s)	Formula	Class
811.4821	10.2	Inf	Unknown	-	-
1016.66462	10.93	Inf	Multiple	$C_{50}H_{98}NO_{17}P$	Phosphosphingolipids
1051.1608	10.17	2919.9	Unknown	-	-
799.48246	10.17	849.5	Unknown	-	-
791.49292	10.17	770.9	Unknown	-	-
833.47629	10.17	622.9	Unknown	-	-
991.67426	10.93	476.3	Unknown	-	-
755.49348	10.93	372.6	Chikusetsusaponin Ia	$C_{41}H_{70}O_{12}$	Steroidal Glycosides
763.48257	10.93	274.1	Unknown	-	-
814.49163	10.2	232.4	Unknown	-	-
766.49126	10.93	210.0	Unknown	-	-
803.49521	10.18	175.6	SQDG(16:0/14:0)	$C_{40}H_{76}O_{12}S$	Glycosyldiacylglycerols
754.9915	10.93	148.1	Unknown	-	-
539.31371	10.17	74.8	Unknown	-	-

531.32451	10.17	66.1	Unknown	-	-
551.31325	10.21	63.1	Neolinderatone or Neolinderachalcone	$C_{35}H_{44}O_4$	Flavonoids
583.29975	10.24	60.6	PG(22:4(7Z,10Z,13Z,16Z)/0:0)	$C_{28}H_{49}O_9P$	Glycerophosphoglycerols
515.31371	10.93	53.2	Unknown	-	-
524.30058	10.93	51.1	Unknown	-	-
547.29899	10.17	35.9	Unknown	-	-
838.49118	10.23	34.7	Unknown	-	-
813.03732	17.02	25.7	Unknown	-	-
444.27975	11.02	24.9	Unknown	-	-
573.30695	10.17	22.5	Unknown	-	-
520.34001	10.17	21.8	Multiple	$C_{26}H_{50}NO_7P$	Glycerophosphocholines
724.43964	12.31	21.5	Unknown	-	-
541.40748	12.43	20.9	Unknown	-	-
783.57384	17.1	20.9	Unknown	-	-
523.34809	10.17	20.0	Unknown	-	-
544.34016	10.23	20.0	Multiple	$C_{28}H_{50}NO_7P$	Glycerophosphocholines
566.32209	10.24	19.4	Multiple	$C_{28}H_{50}NO_7P$	Glycerophosphocholines
539.39103	12.9	19.2	Unknown	-	-
782.57052	17.09	18.4	Multiple	$C_{44}H_{80}NO_8P$	Glycerophosphoethanolamines or Glycerophospholipids
497.34335	10.93	18.2	Unknown	-	-
626.27713	9.47	18.2	Unknown	-	-
803.03827	16.99	17.8	Unknown	-	-
540.31739	10.18	17.6	Unknown	-	-
542.32226	10.17	17.5	Multiple	$C_{26}H_{50}NO_7P$	Glycerophosphocholines

524.3623	11.31	17.3	Unknown	-	-
496.34	10.93	17.2	Multiple	$C_{24}H_{50}NO_7P$	Glycerophosphocholines
534.29657	10.93	16.4	Unknown	-	-
568.34019	10.38	16.4	Multiple	$C_{30}H_{50}NO_7P$	Glycerophosphocholines
590.32244	10.38	16.1	Multiple	$C_{30}H_{50}NO_7P$	Glycerophosphocholines
518.32185	10.93	15.6	Multiple	$C_{24}H_{50}NO_7P$	Glycerophosphocholines
764.53568	11.88	14.6	Unknown	-	-
548.3628	10.72	14.6	Unknown	-	-
568.33818	10.72	13.9	Unknown	-	-
546.34397	11.31	13.7	Unknown	-	-
830.49992	10.64	13.5	Unknown	-	-
526.30455	10.93	13.5	Unknown	-	-
544.33787	11.31	13.2	Multiple	$C_{26}H_{52}NO_7P$	Glycerophosphocholines
658.33594	10.15	13.1	Unknown	-	-
521.32983	10.94	13.1	Unknown	-	-
852.55241	16.88	12.5	Multiple	$C_{50}H_{78}NO_8P$	Glycerophospholipids
291.16958	12.31	12.4	Unknown	-	-
804.55492	16.57	12.4	Multiple	$C_{46}H_{78}NO_8P$	Glycerophosphocholines
367.27659	12.41	12.2	Unknown	-	-
522.35585	11.31	12.0	Multiple	$C_{26}H_{52}NO_7P$	Glycerophosphocholines
419.27163	10.96	11.7	Unknown	-	-
422.25571	16.58	11.7	Unknown	-	-
569.34148	10.71	11.6	Unknown	-	-
968.56647	16.66	11.5	Unknown	-	-
240.09959	10.18	11.5	Unknown	-	-
361.27391	11.89	11.4	Multiple	$C_{23}H_{36}O_3$	Secosteroids
682.04008	12.45	11.3	Unknown	-	-

852.48157	10.64	11.0	Unknown	-	-
588.40043	11.88	11.0	Multiple	$C_{29}H_{60}NO_7P$	Glycerophosphocholines
289.17698	10.93	10.9	Multiple	$C_{16}H_{26}O_3$	Fatty Acids and Conjugates
826.53694	16.58	10.9	Multiple	$C_{48}H_{76}NO_8P$	Glycerophosphocholines
508.33982	10.65	10.8	Multiple	$C_{25}H_{50}NO_7P$	Glycerophosphocholines or Glycerophospholipids
292.14866	10.24	10.8	Unknown	-	-
887.56514	12.3	10.7	Multiple	$C_{47}H_{83}O_{13}P$	Glycosylglycerophospho-lipids
550.30507	10.42	10.6	Unknown	-	-
558.29634	10.43	10.5	Unknown	-	-
363.28926	12.39	10.4	Multiple	$C_{23}H_{38}O_3$	Bile Acids and Derivatives
587.39702	11.88	10.4	Unknown	-	-
680.31787	10.14	10.4	Unknown	-	-
293.15681	10.72	10.2	Unknown	-	-
886.56173	12.31	10.2	Unknown	-	-
548.37157	11.67	10.2	Multiple	$C_{28}H_{55}NO_7P$	Glycerophosphocholines
559.29999	10.44	10.2	PG(20:2(11Z,14Z)/0:0)	$C_{26}H_{49}O_9P$	Glycerophosphoglycerols
478.33004	10.93	10.2	PC(O-16:2(9E,10E)/0:0)[U]	$C_{24}H_{48}NO_6P$	Glycerophosphoethanol-amines or Glycerophosphocholines
284.15957	10.24	10.2	Unknown	-	-
606.30837	11.31	10.1	Unknown	-	-
411.2828	10.96	10.1	Unknown	-	-
508.28291	10.48	10.0	Unknown	-	-
818.51064	16.99	9.9	Unknown	-	-
832.57727	16.87	9.8	Unknown	-	-

277.15406	10.93	9.8	Unknown	-	-
496.3399	10.65	9.7	Multiple	$C_{24}H_{50}NO_7P$	Glycerophosphocholines
908.54341	12.31	9.6	Unknown	-	-
830.57087	16.87	9.5	Multiple	$C_{48}H_{80}NO_8P$	Glycerophosphocholines
846.4638	10.64	9.5	Unknown	-	-
814.04534	17.08	9.5	Unknown	-	-
280.14858	10.17	9.3	Unknown	-	-
281.15647	11.31	8.9	Unknown	-	-
798.09469	18.17	8.9	Unknown	-	-
288.1602	10.93	8.6	Unknown	-	-
272.15969	10.17	8.5	Unknown	-	-
296.14662	10.93	8.3	Unknown	-	-
435.26343	16.88	8.2	Unknown	-	-
272.6661	11.32	8.1	Unknown	-	-
548.275	10.48	8.0	Multiple	$C_{27}H_{44}NO_7P$	Glycerophosphoethanol-amines
293.6626	11.67	8.0	Unknown	-	-
630.30896	10.72	7.9	Unknown	-	-
541.31019	10.17	7.8	Unknown	-	-
473.19758	10.52	7.8	Unknown	-	-
808.58634	17.67	7.7	Multiple	$C_{46}H_{82}NO_8P$	Glycerophosphoethanol-amines or Glycerophosphocholines
549.27846	10.48	7.6	Unknown	-	-
268.1486	10.93	7.5	Unknown	-	-
303.19222	12.31	7.4	Unknown	-	-
920.56633	16.91	7.3	Unknown	-	-

258.6235	10.52	7.3	Unknown	-	-
459.24881	10.93	7.3	Multiple	$C_{21}H_{41}O_7P$	Glycerophosphates or Carbonyl Compounds
409.21932	6.51	6.9	Oleandolide	$C_{20}H_{34}O_7$	Macrolides and Lactone Polyketides
834.50511	16.94	6.9	Multiple	$C_{47}H_{74}NO_8P$	Glycerophosphoethanol-amines
780.55506	17	6.8	Multiple	$C_{44}H_{78}NO_8P$	Glycerophosphoethanol-amines or Glycerophosphocholines
437.27913	17.93	6.8	Unknown	-	-
816.54329	12.35	6.8	Unknown	-	-
792.04419	16.99	6.7	Unknown	-	-
802.53687	17	6.6	Multiple	$C_{46}H_{76}NO_8P$	Glycerophosphocholines or Glycerophosphoethanol-amines
806.57039	17.06	6.6	Multiple	$C_{46}H_{80}NO_8P$	Glycerophosphocholines or Glycerophosphoethanol-amines
858.58972	17.93	6.6	LacCer(d18:0/14:0) or LacCer(d14:0/18:0)	$C_{44}H_{85}NO_{13}$	Neutral Glycosphingolipids
822.5658	16.05	6.5	Multiple	$C_{46}H_{80}NO_9P$	Glycerophosphoserines
282.16423	12.31	6.5	Unknown	-	-
808.57679	17.06	6.4	Unknown	-	-
804.54275	16.99	6.4	Unknown	-	-
280.14876	10.42	6.4	Unknown	-	-
500.31375	16.6	6.3	Unknown	-	-

535.30002	10.94	6.1	PG(18:0/0:0)[U] or PG(18:0/0:0)	$C_{24}H_{49}O_9P$	Glycerophosphoglycerols
628.29241	10.23	6.1	Unknown	-	-
902.52579	12.31	6.0	Unknown	-	-
681.037	12.45	6.0	Unknown	-	-
784.57692	17.11	6.0	Unknown	-	-
447.30305	12.39	5.9	Unknown	-	-
794.57125	17.32	5.8	Unknown	-	-
345.2103	10.72	5.7	Unknown	-	-
571.38293	12.01	5.7	Unknown	-	-
586.31032	10.92	5.7	Unknown	-	-
360.22077	10.17	5.5	Unknown	-	-
802.53704	16.61	5.5	Multiple	$C_{44}H_{78}NO_8P$	Glycerophosphocholines or Glycerophosphoethanol-amines
609.3273	12.3	5.3	Unknown	-	-
856.58386	17.93	5.2	Multiple	$C_{50}H_{82}NO_8P$	Glycerophosphocholines or Glycerophosphoethanol-amines
608.32438	12.31	5.2	Unknown	-	-
580.29259	10.93	5.1	Unknown	-	-
797.6452	19.98	4.9	Unknown	-	-
870.52458	16.99	4.8	Multiple	$C_{47}H_{78}NO_{10}P$	Glycerophosphoserines
341.17874	9.47	4.8	Unknown	-	-
385.27376	11.76	4.7	Unknown	-	-
810.09233	18.13	4.7	Unknown	-	-
604.2927	10.17	4.7	Unknown	-	-

328.28456	12.38	4.6	N-palmitoyl alanine	$C_{19}H_{37}NO_3$	Fatty Amides
652.29294	10.37	4.5	Unknown	-	-
605.29616	10.17	4.4	Multiple	$C_{32}H_{44}O_{11}$	Bufanolides and Derivatives
399.26558	12.15	4.4	10'-Apo-beta-caroten-10'-al or 10'-apo-beta-carotenal	$C_{27}H_{36}O$	Sesterterpenoids
269.22641	12	4.4	Unknown	-	-
478.3293	17	4.4	PC(O-16:2(9E,10E)/0:0)[U] or PE(P-19:1(12Z)/0:0)	$C_{24}H_{48}NO_6P$	Glycerophosphocholines or Glycerophosphoethanol-amines
766.53681	18.33	4.3	Multiple	$C_{43}H_{76}NO_8P$	Glycerophosphocholines or Glycerophosphoethanol-amines
502.32946	17.1	4.3	Unknown	-	-
758.57081	17.52	4.2	Multiple	$C_{42}H_{80}NO_8P$	Glycerophosphocholines or Glycerophosphoethanol-amines
564.3998	12.01	4.1	Unknown	-	-
410.25564	17	4.1	Unknown	-	-
504.32991	12.85	4.1	Unknown	-	-
313.27369	12.45	4.1	Multiple	$C_{19}H_{36}O_3$	Fatty Acids and Conjugates
517.30966	10.93	4.1	Unknown	-	-
341.17862	17	4.0	Unknown	-	-
852.55505	16.34	3.9	Multiple	$C_{50}H_{78}NO_8P$	Glycerophosphocholines
817.51574	11.88	3.9	Unknown	-	-
503.33294	17.11	3.9	Unknown	-	-
745.51501	12.46	3.8	Unknown	-	-

770.06236	17.52	3.8	Unknown	-	-
752.53568	11.88	3.8	Unknown	-	-
753.03777	11.88	3.8	Unknown	-	-
430.40426	8.99	3.7	Unknown	-	-
487.2371	11.76	3.6	Unknown	-	-
428.38861	8.95	3.6	Unknown	-	-
411.26348	17.12	3.4	Unknown	-	-
555.22439	11.76	3.4	Unknown	-	-
213.13076	11.76	3.2	Unknown	-	-
749.54868	19.63	3.2	Ubiquinone 8	$C_{49}H_{74}O_4$	Quinones and Hydroquinones
341.30494	13.77	3.1	Multiple	$C_{21}H_{40}O_3$	Fatty Acids and Conjugates
339.28049	11.88	3.1	Unknown	-	-
406.30313	12.15	3.0	Unknown	-	-
477.43033	16.1	3.0	Unknown	-	-
471.25925	11.76	2.9	Unknown	-	-
795.63005	20.25	2.9	Coenzyme Q9	$C_{54}H_{82}O_4$	Quinones and Hydroquinones
533.34111	11.63	2.9	Unknown	-	-
339.28947	12.81	2.8	Glycidyl oleate	$C_{21}H_{38}O_3$	-
401.22116	11.71	2.8	Unknown	-	-
337.2739	11.88	2.8	Multiple	$C_{21}H_{36}O_3$	Fatty Acids and Conjugates
705.58037	19.8	2.8	Multiple	$C_{40}H_{81}O_7P$	Glycerophosphates
311.25805	11.41	2.8	Multiple	$C_{19}H_{34}O_3$	Fatty Acids and Conjugates
655.56701	19.36	2.7	5-Hydroxy-7-methoxy-2-tritriacontyl-4H-1-benzopyran-4-one	$C_{43}H_{74}O_4$	Benzopyrans
819.61858	20.24	2.7	Unknown	-	-
579.4285	12.95	2.6	Unknown	-	-

953.73405	12.44	2.6	Unknown	-	-
812.65651	20.25	2.6	Unknown	-	-
390.26917	11.88	2.6	Unknown	-	-
367.3358	15.53	2.6	Unknown	-	-
396.31055	12	2.5	Unknown	-	-
575.39681	11.88	2.5	Unknown	-	-
1056.7855	12.8	2.4	Unknown	-	-
461.22143	11.09	2.4	Unknown	-	-
404.28774	11.84	2.4	Unknown	-	-
354.27212	11.05	2.3	Unknown	-	-
335.25819	11.05	2.2	Unknown	-	-

101

Supplementary Table 2. Putative identities of metabolites detected in negative ion mode upregulated in the small intestine of uninfected mice compared with *H. polygyrus*-infected mice.

Untargeted UPLC-FTMS was performed to identify the differential abundance of metabolites in the small intestine of naïve or day 14 *H. polygyrus*-infected 129S1/SvImJ mice. Those metabolites significantly upregulated (p= <0.01) in the small intestine of naïve, compared to *H. polygyrus*-infected mice, that were detected in negative ion mode, are reported. m/z= mass to charge ratio, rt= column retention time, fold= fold change. Putative identities (IDs) were assigned to each metabolite feature where possible.

m/z	rt	fold	Putative ID (s)	Formula	Class
1085.67681	10.17	125.7	Unknown	-	-
654.30631	9.47	28.2	Unknown	-	-
868.6123	18.41	20.9	Unknown	-	-
594.38126	12.54	17.9	Unknown	-	-
246.09946	0.4	17.8	Unknown	-	-
590.33982	10.25	16.9	Unknown	-	-
816.58142	17.83	16.3	Unknown	-	-
590.34974	10.72	16.2	Unknown	-	-
862.56932	12.31	16.1	Unknown	-	-
806.50684	10.65	16.0	Unknown	-	-
553.31668	10.38	15.9	Unknown	-	-
848.5496	16.57	15.8	Unknown	-	-
614.34006	10.38	15.5	Unknown	-	-
504.31245	10.18	13.7	Unknown	-	-

564.33384	10.18	13.2	Unknown	-	-
567.34149	10.17	13.2	Unknown	-	-
658.33804	10.72	13.1	Unknown	-	-
588.334	10.24	12.9	Unknown	-	-
916.53792	16.57	12.7	Unknown	-	-
540.33378	10.93	12.3	Unknown	-	-
480.31206	10.93	12.0	Unknown	-	-
524.33853	10.42	11.4	Unknown	-	-
506.32777	11.31	11.3	Unknown	-	-
602.3056	10.38	11.3	Unknown	-	-
566.34943	11.31	11.0	Unknown	-	-
606.514	17.56	10.9	Unknown	-	-
528.31241	10.26	10.9	Unknown	-	-
874.56549	16.87	10.9	Unknown	-	-
633.51379	12.39	10.7	Unknown	-	-
508.34348	12.31	10.7	Unknown	-	-
634.33739	11.31	10.6	Unknown	-	-
702.32565	11.31	10.3	Unknown	-	-
354.30285	13.32	10.3	Unknown	-	-
556.32084	11.31	10.2	Unknown	-	-
506.3184	10.17	10.2	Unknown	-	-
748.30992	10.37	10.2	Unknown	-	-
568.36515	12.31	10.0	Unknown	-	-
942.55342	16.87	10.0	Unknown	-	-
578.30525	10.24	10.0	Unknown	-	-
529.31567	10.24	10.0	Unknown	-	-
704.24481	10.35	9.9	Unknown	-	-

592.36535	11.67	9.4	Unknown	-	-
424.2806	11.88	9.1	Unknown	-	-
558.33673	12.31	9.0	Unknown	-	-
612.26415	10.93	8.9	Unknown	-	-
840.58067	17.79	8.7	Unknown	-	-
930.55787	12.3	8.6	Unknown	-	-
530.30541	10.93	8.5	Unknown	-	-
554.30573	10.18	8.5	Unknown	-	-
796.55503	11.3	8.3	Unknown	-	-
558.23993	10.35	8.1	Unknown	-	-
423.27725	11.89	8.1	Unknown	-	-
838.56582	17.34	8.0	Unknown	-	-
636.35302	12.31	8.0	Unknown	-	-
592.26879	10.28	8.0	Unknown	-	-
598.21808	5.97	7.6	Unknown	-	-
593.27228	10.29	7.6	Multiple	$C_{27}H_{47}O_{12}P$	Glycerophosphoinositols
844.57426	12.36	7.6	Unknown	-	-
632.32251	10.2	7.6	Unknown	-	-
698.3243	12.3	7.6	Unknown	-	-
422.29093	13.32	7.4	Unknown	-	-
884.56866	17.83	7.1	Unknown	-	-
718.29317	10.24	7.1	Unknown	-	-
856.61173	18.33	7.1	Unknown	-	-
918.55598	16.9	6.8	Unknown	-	-
608.32172	10.93	6.7	Unknown	-	-
568.49778	17.6	6.6	Unknown	-	-
679.49896	11.98	6.5	Unknown	-	-

827.55857	16.98	6.4	Multiple	$C_{43}H_{85}O_{10}P$	Glycerophosphoglycerols
613.25991	10.52	6.4	Unknown	-	-
660.25691	10.29	6.3	Unknown	-	-
670.29283	10.93	6.3	Unknown	-	-
704.34118	12.3	6.2	Unknown	-	-
554.30504	10.44	6.2	Unknown	-	-
885.49483	17.92	5.9	Unknown	-	-
592.26868	10.48	5.6	Unknown	-	-
824.55024	16.99	5.4	Unknown	-	-
878.5967	17.92	5.4	Unknown	-	-
743.54739	18.32	5.4	Unknown	-	-
326.27159	12.37	5.1	Unknown	-	-
742.54401	18.33	4.9	Unknown	-	-
810.53187	18.32	4.7	Unknown	-	-
946.58455	17.93	4.5	Unknown	-	-
494.32784	11.62	4.2	Unknown	-	-
449.28353	11.76	4.0	Multiple	$C_{27}H_{42}O_3$	Secosteroids
475.41797	16.09	3.7	Unknown	-	-
598.29275	10.94	3.7	Unknown	-	-
830.59721	18.17	3.7	Unknown	-	-
447.27744	11.76	3.6	Unknown	-	-
700.31002	10.19	3.5	Unknown	-	-
415.24549	12	3.5	Unknown	-	-
449.29306	12.16	3.4	Unknown	-	-
659.53034	12.79	3.1	Unknown	-	-
375.2769	12.45	3.0	Unknown	-	-
439.24602	11.76	3.0	Unknown	-	-

403.30825	13.79	3.0	Unknown	-	-
373.26118	11.41	3.0	Unknown	-	-
606.23977	10.3	2.9	Unknown	-	-
128.03545	0.42	2.9	Multiple	$C_5H_7NO_3$	Carboxylic Acids and Derivatives
402.29596	12.83	2.9	Unknown	-	-
366.2515	12.44	2.9	Unknown	-	-
639.56118	13.78	2.8	Unknown	-	-
414.25168	11.96	2.8	Unknown	-	-
583.49769	12.43	2.8	Unknown	-	-
534.23955	10.3	2.8	Multiple	$C_{25}H_{42}NO_7P$	Glycerophosphoethanol-amines
655.49867	12.01	2.7	Unknown	-	-
503.27103	7.77	2.7	Unknown	-	-
384.22321	10.01	2.6	Unknown	-	-
365.2689	15.3	2.5	Unknown	-	-
401.29261	12.89	2.5	Unknown	-	-
347.24546	10.97	2.4	Unknown	-	-
401.28266	11.88	2.1	Unknown	-	-
361.26132	11.72	2.1	Unknown	-	-
399.27703	11.89	2.1	Unknown	-	-
348.24885	10.98	2.0	Unknown	-	-

112

113

114

Supplementary Table 3. Putative identities of metabolites detected in positive ion mode upregulated in the small intestine of *H. polygyrus*-infected compared with uninfected mice. Untargeted UPLC-FTMS was performed to identify the differential abundance of metabolites in the small intestine of naïve or day 14 *H. polygyrus*-infected 129S1/SvImJ mice. Those metabolites significantly upregulated (p= <0.01) in the small intestine of *H. polygyrus*-infected, compared to naïve mice, that were detected in positive ion mode, are reported. m/z= mass to charge ratio, rt= column retention time, fold= fold change. Putative identities (IDs) were assigned to each metabolite feature where possible.

m/z	rt	fold	Putative ID (s)	Formula	Class
438.29793	18.34	2179.6	PE(P-16:0/0:0)	$C_{21}H_{44}NO_6P$	Glycerophosphoethanol-amines
566.31331	11.42	33.6	Unknown	-	-
634.53196	17.86	14.9	Unknown	-	-
516.34229	14.21	13.4	PC(P-17:0/0:0) or PE(P-20:0/0:0)	$C_{25}H_{52}NO_6P$	Glycerophosphocholines or Glycerophosphoethanol-amines
451.30583	11.82	12.8	Methyl diacetoxy-10-gingerdiol	$C_{26}H_{42}O_6$	-
566.45479	15.2	11.3	Multiple	$C_{30}H_{64}NO_6P$	Glycerophosphocholines
359.21907	9.21	11.2	Multiple	$C_{20}H_{32}O_4$	Eicosanoids
490.3273	12.92	11.1	Multiple	$C_{23}H_{50}NO_6P$	Glycerophosphocholines or Glycerophosphoethanol-amines
445.2043	4.87	9.9	Multiple	$C_{19}H_{34}O_{10}$	Fatty Acyl Glycosides

514.32658	13.17	9.1	Unknown	-	-
468.34489	12.92	8.8	Multiple	$C_{23}H_{50}NO_6P$	Glycerophosphocholines or Glycerophosphoethanol-amines
950.73035	20.62	8.3	Unknown	-	-
683.48392	18.66	6.9	Unknown	-	-
306.27896	10.3	6.8	Clavepictine B	$C_{20}H_{35}NO$	Sphingoid Bases
359.17209	10.39	5.3	Multiple	$C_{21}H_{24}N_2O_2$	Alkaloids
705.5916	17.35	5.1	SM(d18:0/16:0)	$C_{39}H_{81}N_2O_6P$	Phosphosphingolipids
316.23403	18.65	4.6	Unknown	-	-
480.3221	10.4	3.3	Unknown	-	-
293.17882	12.38	2.6	Unknown	-	-
385.17837	12.3	2.5	17,21-Epoxy-9-fluoro-11beta-hydroxypregn-4-ene-3,20-dione	$C_{21}H_{27}FO_4$	-
318.22772	12.38	2.5	Unknown	-	-
311.18935	12.38	2.4	Unknown	-	-
334.20539	12.38	2.3	Unknown	-	-
627.43465	12.87	2.3	Unknown	-	-
353.21115	12.38	2.2	Methyl (9Z)-8'-oxo-6,8'-diapo-6-carotenoate	$C_{23}H_{28}O_3$	Diterpenoids

124

125

Supplementary Table 4. Putative identities of metabolites detected in negative ion mode upregulated in the small intestine of *H. polygyrus*-infected compared with uninfected mice. Untargeted UPLC-FTMS was performed to identify the differential abundance of metabolites in the small intestine of naïve or day 14 *H. polygyrus*-infected 129S1/SvImJ mice. Those metabolites significantly upregulated (p= <0.01) in the small intestine of *H. polygyrus*-infected, compared to naïve mice, that were detected in negative ion mode, are reported. m/z= mass to charge ratio, rt= column retention time, fold= fold change. Putative identities (IDs) were assigned to each metabolite feature where possible.

m/z	rt	fold	Putative ID (s)	Formula	Class
636.46473	15.23	26.8	Unknown	-	-
606.41807	13.32	25.2	Unknown	-	-
608.43343	14.17	21.3	Unknown	-	-
467.21569	4.87	12.5	Unknown	-	-
403.21211	9.23	12.2	Multiple	$C_{23}H_{32}O_6$	Steroids or Isoprenoids
335.22439	9.23	10.4	Unknown	-	-
582.41743	14.05	10.3	Unknown	-	-
421.21007	4.87	9.6	Unknown	-	-
560.33638	14.21	8.9	PC(18:2(9Z,12Z)/2:0)[U]	$C_{28}H_{52}NO_8P$	Glycerophosphocholines
466.33247	12.93	8.9	Unknown	-	-
516.32559	11.42	7.7	Unknown	-	-
329.12963	10.43	5.2	Unknown	-	-
582.38093	11.72	4.5	Unknown	-	-
363.21707	11.01	3.8	Multiple	$C_{21}H_{32}O_5$	Steroids

223.17117	10.22	3.1	Unknown	-	-
323.26074	12.33	2.5	Unknown	-	-

135